JACS
JOURNAL OF THE AMERICAN CHEMICAL SOCIETY

ARTICLE

pubs.acs.org/JACS

Hexadentate Terephthalamide(bis-hydroxypyridinone) Ligands for Uranyl Chelation: Structural and Thermodynamic Consequences of Ligand Variation[1]

Géza Szigethy and Kenneth N. Raymond*

Department of Chemistry, University of California at Berkeley, Berkeley, California 94720-1460, United States

Chemical Sciences Division, Glenn T. Seaborg Center, Lawrence Berkeley National Laboratory, Berkeley, California 94720, United States

Supporting Information

ABSTRACT: Several linear, hexa- and tetradentate ligands incorporating a combination of 2,3-dihydroxy-terephthalamide (TAM) and hydroxypyridinone-amide (HOPO) moieties have been developed as uranyl chelating agents. Crystallographic analysis of several $\{UO_2[TAM(HOPO)_2]\}^{2-}$ complexes revealed a variable and crowded coordination geometry about the uranyl center. The TAM moiety dominates the bonding in hexadenate complexes, with linker rigidity dictating the equality of equatorial U−O bonding. Hexadentate TAM-$(HOPO)_2$ ligands demonstrated slow binding kinetics with uranyl affinities on average 6 orders of magnitude greater than those of similarly linked bis-HOPO ligands. Study of tetradentate TAM(HOPO) ligands revealed that the high uranyl affinity stems primarily from the presence of the TAM moiety and only marginally from increased ligand denticity. Uranyl affinities of $TAM(HOPO)_2$ ligands were within experimental error, with TAM-(*o*-phen-1,2-HOPO)$_2$ exhibiting the most consistent uranyl affinity at variable pH.

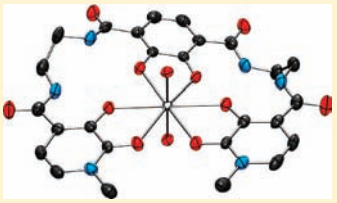

INTRODUCTION

The uranyl cation (UO_2^{2+}) and the related dioxo cations (actinyls, AnO_2^{n+}, where An = U, Np, Pu, and n = 1, 2) pose an unusual challenge for the rational design of selective sequestering agents.[2,3] These complications stem partly from the trans orientation of their oxo atoms, which relegate ligand coordination to an equatorial plane perpendicular to the O═An═O vector; significant deviations from actinyl linearity[4−7] or equatorial coordinative planarity[5,8] occur only in the presence of unusually sterically demanding ligands. Additionally, the actinyl oxo moieties generally exhibit poor Lewis basicity, and interactions between oxo groups and Lewis acids are typically only observed in the solid state,[9−15] in carefully designed ligand scaffolds,[6,16−19] or with the lower-valent actinyls due to the decreased Lewis acidity of the central actinide.[20−22] As a result, few actinyl chelating agents attempt targeted interaction with the oxo moieties,[18,19,23] with most instead focusing on optimizing bonding interactions in the equatorial coordination plane.[24] As a natural example for the efficacy of equatorial chelation, oceanic uranium exists as the $[UO_2(CO_3)_3]^{4-}$ complex, with extremely low concentrations of the uncoordinated uranyl cation (1.53×10^{-17} M).[25]

A special class of ligands investigated as high-denticity *f*-element chelators are macrocycles, the design strategies for which are discussed in several comprehensive reviews.[26−29] Macrocycles targeted toward *f*-elements are by and large applied toward lanthanide(III) chelation, with ring sizes of 18 atoms and higher. However, they are often incapable of providing coordinative saturation to lanthanide(III) cations due to insufficient coordinating atoms and limited flexibility. These structural limitations make macrocycles better suited to the coordinative inflexibility about actinyl cations. Macrocyclic actinyl complexes are plentiful and coordinative saturation can be achieved with conveniently placed O-, N-, and S-donating groups in both flexible and rigid penta- and hexadenate macrocycles.[8,26,27,30,31] The drawback to macrocyclic chelating agents, however, is that their ligand conformation may be sensitive to steric agreement between binding pocket and chelated ion, requiring a careful approach to target ligand design.[8]

Our recent work on actinyl-specific sequestering agents has addressed the incorporation of siderophore-inspired catechol-amide (CAM), 2,3-dihyroxy-terephthalamide (TAM), and hydroxypyridinone-amide (HOPO) binding moieties into polybidentate, equatorially coordinating ligands.[3,32−34] These hard Lewis basic chelating moieties are well-suited for binding the Lewis acidic actinyls, and several studies exist on their crystallographic, thermodynamic, and in vivo actinide decorporation properties.[3,33−36] These analyses indicated that bis-bidentate ligands more effectively chelate the uranyl cation than monobidentate ligands. However, recent studies suggested that bis-bidentate siderophore-inspired ligands fail to saturate the uranyl coordination plane, leaving a solvent-accessible area at the uranium center whose size is inversely proportional to linker length (Figure 1).[32−34] While typically occupied by solvent molecules, this open coordination site could allow undesired interactions between the exposed uranyl center and the environment from which it is being extracted via coordination of

Received: February 17, 2011
Published: May 04, 2011

dx.doi.org/10.1021/ja201511u | *J. Am. Chem. Soc.* 2011, 133, 7942–7956

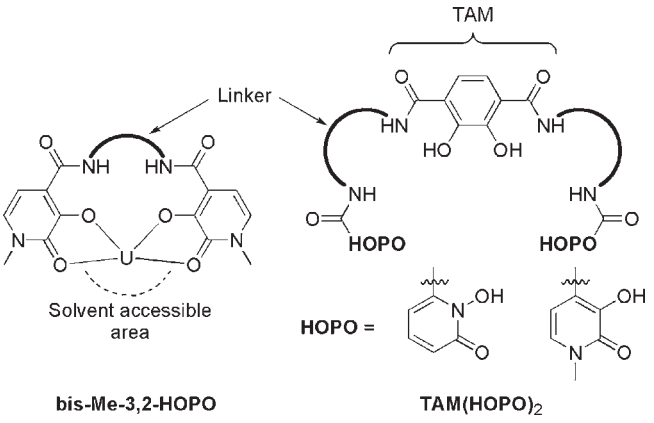

Figure 1. (Left) Solvent accessible area in UO_2(bis-Me-3,2-HOPO) complexes (uranyl oxo atoms omitted for clarity). (Right) Tris-bidentate ligand design for coordinative saturation of actinyl cations.

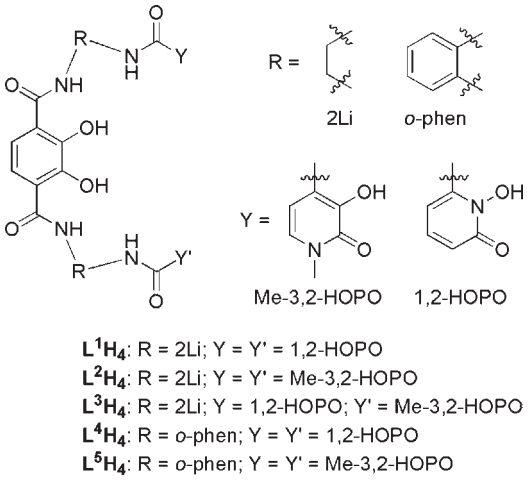

Figure 2. Hexadentate TAM(HOPO)$_2$ ligands.

mono- or bidentate ligands (e.g., hydroxide or acetate; bite angle of 52°).[37] The typical 66° bite angle of catecholates/hydroxypyridinones at the uranyl center[33,34,38,39] explains the lack of a known uranyl complex saturated by three such moieties, but it was surmised that a tris-bidentate ligand could achieve coordinative saturation by strategic employment of appropriately shaped linker molecules.[40] Such a ligand could capitalize upon coordinative saturation observed in macrocyclic uranyl complexes without the geometric constraints imparted by a rigidly defined coordination pocket

The hexadentate ligand design employed in this study incorporates three bidentate, oxygen-donating TAM and HOPO chelating moieties [TAM(HOPO)$_2$ ligands, Figure 1]. This ligand geometry is similar to the macrocyclic and linear ligands of Nabeshima and co-workers,[41−43] as well as the macrocycles developed by MacLachlan,[44] which have collectively been shown to bind both transition and lanthanide metal cations. In contrast to Schiff base macrocycles, the amide linkages employed in Figure 1 allow only catecholate-type binding modes due to the presence of amide protons which are known to stabilize the negative charge of deprotonated *o*-phenolate oxygens via intramolecular hydrogen bonding.[45] Macrocyclic tris-catecholamide ligands have been synthesized and investigated by our group as Fe(III) chelators,[46] but the linear ligand design in Figure 1 is intended to provide a greater level of coordinative flexibility than that in macrocycles. This flexibility is ideal for the current study because the steric consequences of uranyl chelation by synthetic, hexadentate siderophore ligands are as yet unexplored. The work discussed herein details the characterization of the solid-state and solution-phase interactions of TAM(HOPO)$_2$ ligands with the uranyl cation.

RESULTS AND DISCUSSION

Hexadentate Ligand Design. Two properties of the TAM moiety make it ideal for inclusion in the ligand topology in Figure 1: (1) the presence of two amide groups allows it to act as a functional ligand extension (whereas the HOPO moiety can only act as a terminal group), and (2) TAM is known to form strong complexes with hard Lewis acidic ions such as Fe(III)[47] and Th(IV).[48] The terminal binding moieties in Figure 1 were chosen to be HOPO moieties for two reasons: (1) they exhibit lower acidity than the TAM moiety,[35,47] helping the ligands bind at lower pH, and (2) they are monoprotic, resulting in dianionic uranyl complexes as opposed to the tetraanionic species that would result with a tris-TAM ligand.

Alkyl-linked TAM(HOPO)$_2$ ligands have been previously explored as high-affinity Fe(III) chelating agents and are capable of adopting octahedral coordination geometries about Fe(III) when the linkers contain three or more methylene units.[49] However, the capacity for octahedral coordination is undesirable in ligands designed for the purely equatorial coordination preferences of actinyl cations, suggesting the use of linkers with no more than two carbon atoms between the amide nitrogens. The shortest linkers observed in mononuclear bis-HOPO uranyl complexes are 3,4-thiophene-, *o*-phenylene-, and ethylenediamine (2Li; "Li" indicating a linear alkyl linker containing two methylene units). These linkers also provided the largest solvent accessible area about the uranyl cation in bis-Me-3,2-HOPO structures, making them appropriate linkers for actinyl-specific TAM(HOPO)$_2$ ligands.[33] On the basis of these observations, ligands $\mathbf{L^1H_4}$−$\mathbf{L^5H_4}$ were designed to incorporate *o*-phenylene- and ethylenediamine linkers and both the 1,2- and Me-3,2-HOPO moieties as terminal bidentate units (Figure 2). $\mathbf{L^1H_4}$ through $\mathbf{L^5H_4}$ are amorphous, beige solids that exhibit poor solubility in water and most organic solvents with the exception of DMF and DMSO. Deprotonation makes them significantly more soluble in polar, organic solvents, although the *o*-phenylene-linked ligands, $\mathbf{L^4H_4}$ and $\mathbf{L^5H_4}$, exhibit much lower solubility than the 2Li-linked ligands $\mathbf{L^1H_4}$−$\mathbf{L^3H_4}$. Ligands containing the 1,2-HOPO moiety exhibit slightly better solubility than those containing the Me-3,2-HOPO moiety, independent of solvent choice or degree of protonation.

Synthesis and Structure of Uranyl Complexes. Mononuclear $\{UO_2[TAM(HOPO)_2]\}^{2-}$ complexes were synthesized in either DMF or methanol using a combination of KOH and NMe_4OH as bases. The use of hydroxide bases ensured complete ligand deprotonation, since alkyl-substituted TAM moieties exhibit second pK_a values of 10.3−11.0.[47] Unlike the orange or red color of uranyl complexes with tetradentate bis-Me-3,2-HOPO ligands,[32−35] $\{UO_2[TAM(HOPO)_2]\}^{2-}$ complexes are dark brown in solution and in the solid state, independent of HOPO moiety and linker geometry. Because they are dianionic and thus highly soluble, the uranyl complexes are difficult to separate from the mixture of potassium, tetramethylammonium,

dx.doi.org/10.1021/ja201511u |*J. Am. Chem. Soc.* 2011, 133, 7942–7956

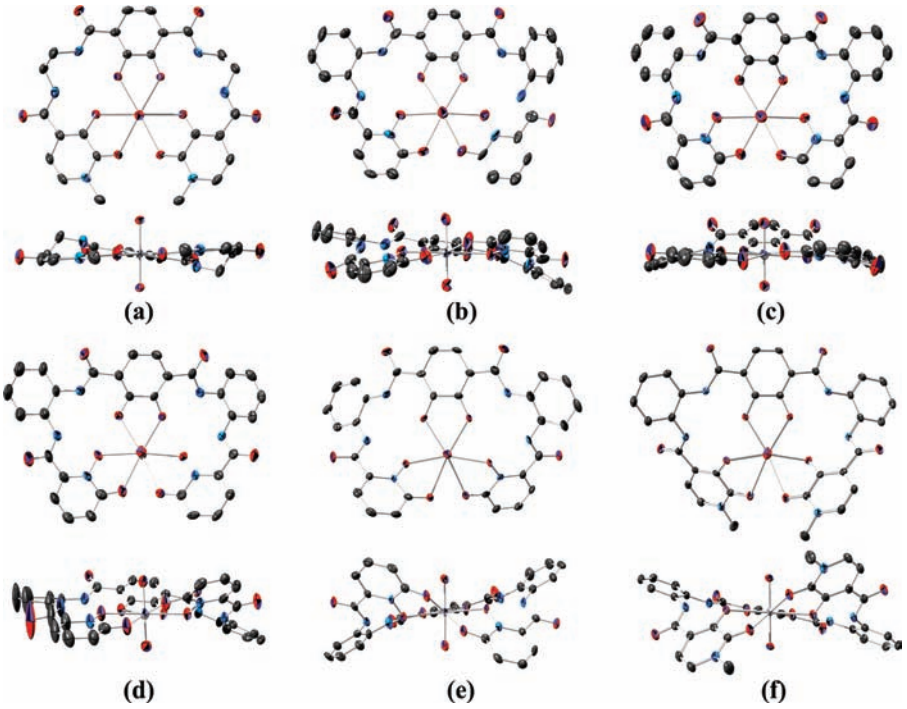

Figure 3. Top and side views of X-ray diffraction structures of $\{UO_2[TAM(HOPO)_2]\}^{2-}$ complexes: (a) $[UO_2(\mathbf{L^2})]^{2-}$; (b–e) $[UO_2(\mathbf{L^4})]^{2-}$ #1–#4 respectively; (f) $[UO_2(\mathbf{L^5})]^{2-}$. Thermal ellipsoids are drawn at the 50% probability level. Hydrogen atoms, counterions, and solvent molecules are omitted for clarity. Oxygen atoms are red, carbons gray, nitrogens blue, and uranium is silver.

and nitrate salts that are byproducts of their complexation. Clean isolation of $\{UO_2[TAM(HOPO)_2]\}^{2-}$ complexes was afforded in most cases by solvent layering or vapor diffusion techniques that selectively deposited the uranyl complexes, often in crystalline form. Isolation of crystalline, X-ray-quality samples of $[UO_2(\mathbf{L^2})]^{2-}$, $[UO_2(\mathbf{L^4})]^{2-}$, and $[UO_2(\mathbf{L^5})]^{2-}$ was facilitated by the poor solubility imparted by the Me-3,2-HOPO moieties and the *o*-phenylene linkers, whereas crystals of $[UO_2(\mathbf{L^1})]^{2-}$ and $[UO_2(\mathbf{L^3})]^{2-}$ could not be cleanly isolated. The six crystal structures collected from these samples (one each of $[UO_2(\mathbf{L^2})]^{2-}$ and $[UO_2(\mathbf{L^5})]^{2-}$, and four of $[UO_2(\mathbf{L^4})]^{2-}$) are shown in Figure 3, with crystallographic parameters listed in Table 1.

The $TAM(HOPO)_2$ ligands bind the uranyl cation in a hexadentate fashion, with all coordinating oxygens occupying the equatorial coordination plane. This behavior is independent of HOPO moiety or linker rigidity, although there exists a variable amount of ligand ruffling out of the coordination plane which differs even between the four structure of $[UO_2(\mathbf{L^4})]^{2-}$. We suggest that the inclusion of the third bidentate moiety is responsible for the observed ligand distortions, since tetradentate bis-HOPO ligands utilizing similar linkers adopt very planar coordination modes about the uranyl cation.[33]

To better understand the bonding in $\{UO_2[TAM(HOPO)_2]\}^{2-}$ complexes, comparison against uranyl complexes with analogous tetradentate bis-HOPO ligands was required. Appropriate tetradentate analogues for $\mathbf{L^2H_4}$, $\mathbf{L^4H_4}$, and $\mathbf{L^5H_4}$ are 2Li-Me-3,2-HOPO [(**2Li32HP**)H_2],[34] *o*-phenylene-1,2-HOPO [(**phen12HP**)H_2],[50] and *o*-phenylene-Me-3,2-HOPO [(**phen32HP**)H_2],[33] respectively (Figure 4). The UO_2(**2Li32HP**) and UO_2(**phen32HP**)(DMSO) complexes have been reported,[33] and the UO_2(**phen12HP**)(DMSO) complex was synthesized following standard synthetic procedures [the UO_2(**phen12HP**)(DMSO) crystal structure and crystallographic parameters are provided in the Supporting Information].[34] Typical of UO_2(bis-Me-3,2-HOPO) complexes, $(\mathbf{phen12HP})^{2-}$ binds uranyl with four oxygen atoms in the equatorial coordination plane, with coordinative saturation provided by a molecule of DMSO.[33,34]

The equatorial U–O bond lengths in the $\{UO_2[TAM(HOPO)_2]\}^{2-}$ and UO_2(bis-HOPO) complexes are labeled schematically in Figure 5 and are compared in Table 2. Although the bond lengths vary significantly between the investigated structures, the $U-O_{TAM}$ distances in the hexadentate structures are very similar, with an average of about 2.40(3) Å. This bond distance is consistent with the 2.39–2.49 Å M–O bond lengths in $[ML_4]^{4-}$ complexes, where M is U/Th(IV) and L is a bidentate, untethered TAM or catechol.[48,51] The invariance in $U-O_{TAM}$ bond lengths suggests that the TAM moiety dominates the chelation behavior in $\{UO_2[TAM(HOPO)_2]\}^{2-}$ complexes.

In tetradentate bis-HOPO uranyl complexes the $U-O_{phenolate}$ bond lengths are typically about 0.1 Å shorter than the $U-O_{amide}$ bond lengths, as observed in UO_2(**2Li32HP**) and UO_2(**phen32HP**)(DMSO). This is consistent with a stronger U–O bond to the more negatively charged phenolate oxygen than to the neutral amide oxygen.[33,34] However, the $U-O_{HOPO}$ distances in the hexadentate $[UO_2(\mathbf{L^2})]^{2-}$ complex are nearly equal, and both are longer than the $U-O_{amide}$ bonds in UO_2(**2Li32HP**) by 0.1 Å. This suggests that the geometric constraints of hexadentate uranyl coordination require a sacrifice in bond strength to the HOPO oxygens even when utilizing the flexible 2Li linker. The constraints of uranyl chelation also generate a mild helical twist in $[UO_2(\mathbf{L^2})]^{2-}$, indicating that fully planar coordination is not quite achievable given the bite angles and geometric constraints of the $TAM(HOPO)_2$ ligand design.

In contrast to the mild ligand distortion in $[UO_2(\mathbf{L^2})]^{2-}$, the four $[UO_2(\mathbf{L^4})]^{2-}$ structures exhibit a wide variety of ligand

dx.doi.org/10.1021/ja201511u |*J. Am. Chem. Soc.* 2011, 133, 7942–7956

Table 1. Crystallographic Parameters for $\{UO_2[TAM(HOPO)_2]\}^{2-}$ Complexes

	$[UO_2L^2]^{2-}$	$[UO_2L^4]^{2-}$, #1	$[UO_2L^4]^{2-}$, #2	$[UO_2L^4]^{2-}$, #3	$[UO_2L^4]^{2-}$, #4	$[UO_2L^5]^{2-}$
formula	$C_{26}H_{24}N_6O_{12}U\cdot 2(C_4H_{12}N)\cdot 2(C_3H_6O)$	$C_{20}H_{20}N_6O_{12}U\cdot 2(C_4H_{12}N)\cdot CH_4O\cdot 4.35(C_4H_8O_2)\cdot 0.15(C_2H_6OS)$	$C_{32}H_{20}N_6O_{12}U\cdot 2(C_4H_{12}N)\cdot 2(C_4H_8O_2)\cdot C_2H_6OS$	$C_{32}H_{20}N_6O_{12}U\cdot 2(C_4H_{12}N)\cdot 3(H_2O)\cdot CH_4O\cdot 3(C_4H_8O_2)\bullet$	$C_{32}H_{20}N_6O_{12}U\cdot 2(C_4H_{12}N)\cdot C_2H_6OS$	$C_{34}H_{24}N_6O_{12}U\cdot 2(C_4H_{12}N)\cdot 2(CH_4O)$
MW	1114.99	1493.88	1321.20	1417.26	1144.99	1159.00
T [K]	144(2)	154(2)	103(2)	163(2)	135(2)	152(2) K
crystal system	tetragonal	triclinic	orthorhombic	triclinic	triclinic	monoclinic
space group	$P4_12_12$	$P\bar{1}$	*Pbca*	$P\bar{1}$	$P\bar{1}$	*C2/c*
habit	wedge	plate	prism	plate	plate	rhombohedron
color	red	brown	brown	yellow	yellow	red
a[Å]	17.686(3)	9.7996(14)	17.625(4)	9.2600(15)	9.6429(14)	16.970(2)
b[Å]	17.686(3)	17.047(2)	23.731(5)	13.259(2)	13.330(2)	12.5873(18)
c [Å]	14.605(3)	19.030(3)	26.021(5)	23.405(4)	18.927(4)	22.161(3)
α [deg]	90	102.075(2)	90	79.417(2)	110.241(3)	90
β [deg]	90	95.478(3)	90	86.227(2)	102.292(3)	108.948(2)
γ [deg]	90	91.560(3)	90	88.558(2)	93.606(2)	90
V [Å^3]	4568.6(13)	3090.8(8)	10883(4)	2818.3(8)	2205.4(6)	4477.2(11)
Z	4	2	8	2	2	4
ρ_{calcd} [g cm^{-3}]	1.621	1.605	1.613	1.670	1.724	1.719
μ_{palcd} [mm^{-1}]	3.626	2.716	3.099	2.968	3.802	3.703
θ range [°]	2.30, 26.39	2.26, 21.32	3.41, 25.38	3.30, 24.78	2.53, 25.90	2.53, 26.38
total reflections	26113	12833	49048	14330	15258	12451
data/restr./ param.	4687/0/292	6860/171/782	9927/142/720	9212/6/582	7927/6/623	4576/0/310
F(000)	2240	1522	5328	1440	1140	2320
T_{min}/T_{max}	0.787	0.798	0.538	0.582	0.557	0.656
cryst. size [mm^3]	0.18 × 0.14 × 0.10	0.12 × 0.08 × 0.03	0.32 × 0.12 × 0.07	0.23 × 0.09 × 0.02	0.20 × 0.07 × 0.02	0.16 × 0.10 × 0.03
R1[$I>2\sigma(I)$][a]	0.0298	0.0538	0.0331	0.0479	0.0486	0.0253
wR2 (all data)[a]	0.0638	0.1364	0.0842	0.1106	0.1263	0.0580
GOF[a]	1.032	1.029	1.214	0.940	1.017	1.057

[a] $R1 = \Sigma||F_o| - |F_c||/\Sigma|F_o|$; $wR2 = [\Sigma[w(F_o^2 - F_c^2)^2]/\Sigma[w(F_o^2)^2]]^{1/2}$; $GOF = [\Sigma w(|F_o| - |F_c|)^2/(n-m)]^{1/2}$.

dx.doi.org/10.1021/ja201511u | *J. Am. Chem. Soc.* 2011, 133, 7942–7956

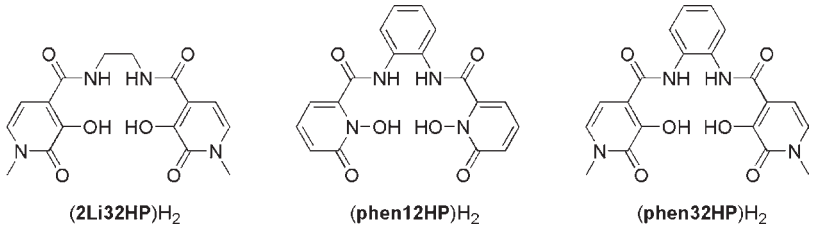

Figure 4. Tetradentate ligands for structural comparison of uranyl complexes.[33,34,50]

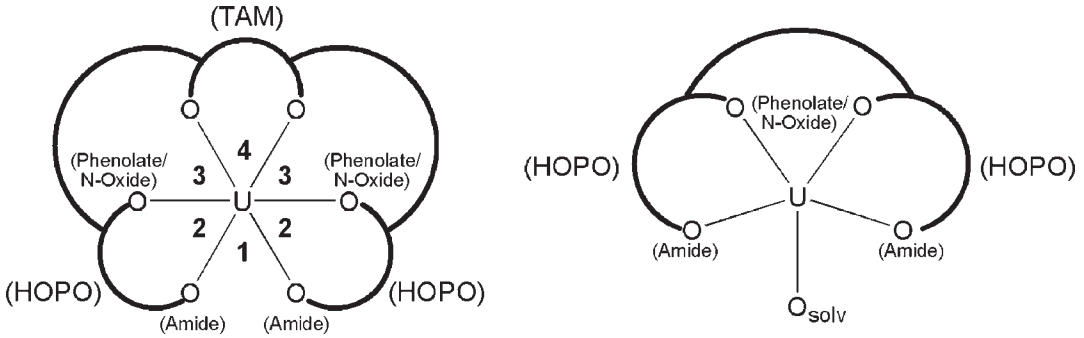

Figure 5. Schematic of equatorial U−O bond lengths, angles, and binding pocket layout in uranyl complexes with TAM(HOPO)$_2$ and bis-Me-3,2-HOPO ligands.

Table 2. Equatorial U−O Bond Lengths in $\{UO_2[TAM(HOPO)_2]\}^{2-}$ and UO_2(bis-HOPO) Complexes Labeled According to Figure 5[c]

Complex	U–O (HOPO amide), [Å]	U–O (HOPO phenolate/ N-oxide), [Å]	U–O (TAM), [Å]
$[UO_2(\mathbf{L^2})]^{2-}$	2.544(3)[a]	2.528(3)[a]	2.405(3)[a]
UO_2(**2Li32HP**) [33]	2.442(8), 2.471(8)	2.301(7), 2.383(7)	N/A
$[UO_2(\mathbf{L^4})]^{2-}$, #1	2.460(7), 2.508(7)	2.533(7), 2.551(7)	2.384(6), 2.428(7)
$[UO_2(\mathbf{L^4})]^{2-}$, #2	2.416(3), 2.449(3)	2.590(3), 2.607(3)	2.387(3), 2.407(3)
$[UO_2(\mathbf{L^4})]^{2-}$, #3	2.443(5), 2.535(4)	2.484(4), 2.517(4)	2.370(4), 2.446(4)
$[UO_2(\mathbf{L^4})]^{2-}$, #4	2.552(6), 2.558(5)	2.410(5), 2.417(5)	2.353(5), 2.403(5)
UO_2(**phen12HP**)(DMSO)	2.341(6), 2.371(6); 2.361(6), 2.370(6)[b]	2.374(5), 2.375(5); 2.345(6), 2.367(6)[b]	N/A
$[UO_2(\mathbf{L^5})]^{2-}$	2.730(2)[a]	2.419(2)[a]	2.403(2)[a]
UO_2(**phen32HP**)(DMSO) [33]	2.446(3), 2.458(3)	2.330(3), 2.349(3)	N/A

[a] The two halves of the molecule are crystallographically identical. [b] Two unique uranyl complexes exist in the asymmetric unit. [c] Tetradentate complexes are listed in shaded cells.

orientations about the uranyl cation. In $[UO_2(\mathbf{L^4})]^{2-}$ structures #1 and #4 (Figure 3b and e), helical twists similar to that in $[UO_2(\mathbf{L^2})]^{2-}$ are observed, while in $[UO_2(\mathbf{L^4})]^{2-}$ structures #2 and #3 (Figure 3c and d), the TAM moiety bends completely to one side of the uranyl coordination plane. A range of U−O_{HOPO} bond distances accompany these ligand distortions (intermolecular Δd_{max} = 0.2 Å). However, all of the U−O_{HOPO} bonds in $[UO_2(\mathbf{L^4})]^{2-}$ are 0.1−0.2 Å longer than in the tetradentate UO_2(**phen12HP**)(DMSO) complex, in which the U−O_{amide} and U−$O_{N\text{-}oxide}$ bonds are nearly identical. The U−O_{amide} and U−$O_{N\text{-}oxide}$ bond equality in UO_2(**phen12HP**)(DMSO) is in fact typical of coordination complexes of 1,2-HOPO with cations such as Fe(III), Co(III), UO_2^{2+} and Th(IV), in which M−$O_{N\text{-}oxide}$ and M−O_{amide} bonds are the same to within 0.03 Å.[38,52,53] This is due to a resonance form of the deprotonated 1,2-HOPO moiety that populates the formally neutral amide oxygen with negative charge and establishes aromaticity. Such a resonance form is insignificant in the Me-3,2-HOPO moiety, given the propensity for M−$O_{phenolate}$ bonds to be shorter than M−O_{amide} bonds in complexes with the Me-3,2-HOPO ligand.[33,34,54−58] Surprisingly, the hexadentate $[UO_2(\mathbf{L^4})]^{2-}$ structures #1−#3 display U−$O_{N\text{-}oxide}$ bond lengths that are actually longer than their U−O_{amide} bonds. In addition, the U−$O_{N\text{-}oxide}$ bonds vary up to 0.18 Å within each complex. As in $[UO_2(\mathbf{L_2})]^{2-}$, these bond distances are considered to be the result of geometric constraints imposed by the TAM-dominated chelation with the additional constraints of the *o*-phenylene linker rigidity.

The $[UO_2(\mathbf{L^5})]^{2-}$ structure displays a severe helical ligand twist similar to that in $[UO_2(\mathbf{L^2})]^{2-}$ and $[UO_2(\mathbf{L^4})]^{2-}$ structures #1 and #4. The U−$O_{phenolate}$ bond length is comparable to

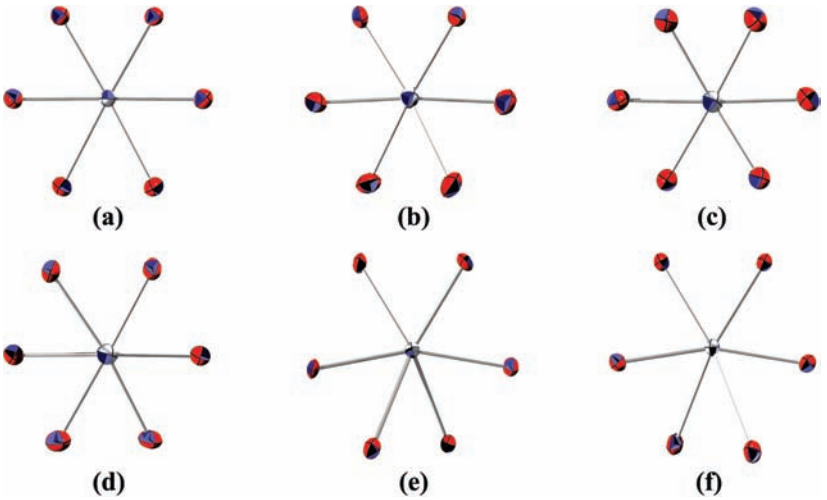

Figure 6. Uranyl binding pockets in $\{UO_2[TAM(HOPO)_2]\}^{2-}$ complexes with ligands: (a) $(\mathbf{L^2})^{4-}$; (b)−(e) $(\mathbf{L^4})^{4-}$, #1−#4 respectively; (f) $(\mathbf{L^5})^{4-}$. Structures are viewed down the uranyl O═U═O vector, with uranyl oxo atoms omitted for clarity. Oxygen atoms are oriented as illustrated in Figure 5. Thermal ellipsoids are drawn at the 50% probability level. Oxygen atoms are red and uraniums are silver.

Table 3. Equatorial O−U−O Bite Angles in $\{UO_2[TAM(HOPO)_2]\}^{2-}$ Complexes; Angle Labels Refer to Those in Figure 5

complex	angle 1, [deg]	angle 2, [deg]	angle 3, [deg]	angle 4, [deg]	angle sum, [deg]
$[UO_2\mathbf{L^2}]^{2-}$	57.9(1)[a]	60.9(1)[a]	59.6(1)[a]	63.3(1)[a]	362.2(2)[a]
$[UO_2\mathbf{L^4}]^{2-}$, #1	59.0(3)	59.8(2), 60.7(2)	59.4(2), 60.8(2)	65.0(2)	364.7(5)
$[UO_2\mathbf{L^4}]^{2-}$, #2	60.5(1)	59.3(1), 59.9(1)	58.87(9), 59.25(9)	64.4(1)	362.2(2)
$[UO_2\mathbf{L^4}]^{2-}$, #3	60.0(2)	60.5(1), 61.1(2)	60.2(1), 62.9(1)	64.3(1)	369.0(3)
$[UO_2\mathbf{L^4}]^{2-}$, #4	64.3(2)	59.4(2), 60.7(2)	66.6(2), 67.5(2)	65.2(2)	383.7(5)
$[UO_2\mathbf{L^5}]^{2-}$	59.58(9)[a]	60.71(6)[a]	65.93(7)[a]	65.40(9)[a]	378.3(2)[a]

[a] The two halves of the molecule are crystallographically identical, giving rise to single values for angles 2 and 3.

those in the other $\{UO_2[TAM(HOPO)_2]\}^{2-}$ structures, but the $U-O_{amide}$ distance of 2.7 Å is longer even than those of uranyl-coordinated DMSO or DMF molecules (typically about 2.4 Å), suggesting a very weak interaction with the HOPO amide oxygen atoms.[33,34] This disparity in $U-O_{HOPO}$ bond lengths is again evidence that the TAM moiety dominates the binding interaction between the uranyl cation and $TAM(HOPO)_2$ ligands.

The tendency for uranyl complexes with ligands $(\mathbf{L^4})^{4-}$ and $(\mathbf{L^5})^{4-}$ to exhibit more pronounced ligand distortions than those with $(\mathbf{L^2})^{4-}$ suggests that the *o*-phenylene linker imposes too much steric constraint for unhindered uranyl chelation. The gauche conformation of the linear 2Li linker may explain the relatively small deviation from planarity in the $[UO_2(\mathbf{L^2})]^{2-}$ structure; this natural alkyl conformation allows a closer approach of the HOPO moieties to the uranyl center than does the rigid *o*-phenylene linker. Figure 6 illustrates the effect ligand rigidity has on uranyl position in the $TAM(HOPO)_2$ binding pocket: the ethylene-linked $(\mathbf{L^2})^{4-}$binds the uranium most equally, while the *o*-phenylene linked $(\mathbf{L^4})^{4-}$ and $(\mathbf{L^5})^{4-}$ bind the uranium atom farther back toward the TAM moiety, with $U-O_{TAM}$ and $U-O_{HOPO}$ bond lengths becoming more unequal with increasing helical ligand twist (Figure 6e and f).

Additional information on the interaction between UO_2^{2+} and $TAM(HOPO)_2$ ligands can be gleaned from the equatorial O−U−O angles listed in Table 3. The HOPO bite angle (angle 2) is constant at about 60° in all $\{UO_2[TAM(HOPO)_2]\}^{2-}$ structures, which is approximately 6° smaller than in uranyl complexes with mono- and bis-bidentate 1,2- and Me-3,2-HOPO ligands.[33,34,38] The decrease in bite angle is caused by the relatively long equatorial $U-O_{HOPO}$ bond distances discussed above. In contrast, the TAM bite angles range between 63° and 65°, which are closer to the 65° TAM bite angle in the unconstrained $[Th(ETAM)_4]^{4-}$,consistent with the above conclusion that the TAM moiety dominates the binding event in $\{UO_2[TAM(HOPO)_2]\}^{2-}$ complexes.[48]

The total equatorial angle sum in the uranyl complexes is a metric by which coordinative crowding can be assessed. This sum is ideally 360° for completely planar coordination and is expected to increase upon coordinative crowding, which would in turn be suggestive of poor geometric agreement between the uranyl cation and coordinated ligands. Equatorial angle sums in uranyl complexes deviate little from 360° when using mono- and bidentate ligands, but may do so much more in the presence of macrocyclic or coordinatively saturating ligands. The $[UO_2(\mathbf{L^2})]^{2-}$ structure exhibits the smallest angle sum of 362°, but upon exchanging the flexible 2Li linker for the rigid *o*-phenylene in $(\mathbf{L^4})^{4-}$ and $(\mathbf{L^5})^{4-}$, the angle sums generally increase, with a maximum of 384° observed in $[UO_2(\mathbf{L^4})]^{2-}$ structure #4. These deviations illustrate the significant geometric strain the *o*-phenylene linkers introduce to the $\{UO_2[TAM(HOPO)_2]\}^{2-}$ complexes which the 2Li linker in $(\mathbf{L^2})^{4-}$ more effectively mitigate.

The interplanar TAM/HOPO/uranyl angles listed in Table 4 yield additional information about the details of uranyl chelation

dx.doi.org/10.1021/ja201511u |*J. Am. Chem. Soc.* 2011, 133, 7942–7956

Table 4. Interplanar Angles in $\{UO_2[TAM(HOPO)_2]\}^{2-}$ Complexes

complex	HOPO−HOPO [deg]	HOPO−TAM [deg]	HOPO−uranyl [deg]	TAM−uranyl [deg]
$[UO_2\mathbf{L^2}]^{2-}$	2.5(3) [a]	12.3(2) [a]	3.8(2) [a]	8.7(2) [a]
$[UO_2\mathbf{L^4}]^{2-}$, #1	30.8(5)	16.4(5), 25.9(5)	13.9(5), 17.0(4)	16.9(4)
$[UO_2\mathbf{L^4}]^{2-}$, #2	14.9(2)	23.2(1), 37.5(1)	5.1(1), 13.1(2)	24.54(8)
$[UO_2\mathbf{L^4}]^{2-}$, #3	45.3(2)	11.6(3), 56.6(2)	17.8(2), 27.6(2)	29.0(2)
$[UO_2\mathbf{L^4}]^{2-}$, #4	81.8(2)	46.0(3), 49.0(2)	41.9(2), 44.5(2)	11.4(3)
$[UO_2\mathbf{L^5}]^{2-}$	71.49(8) [a]	48.3(1) [a]	41.1(1) [a]	13.1(2) [a]

[a] The two halves of the molecule are crystallographically identical, giving rise to only one HOPO−TAM and HOPO−uranyl angle.

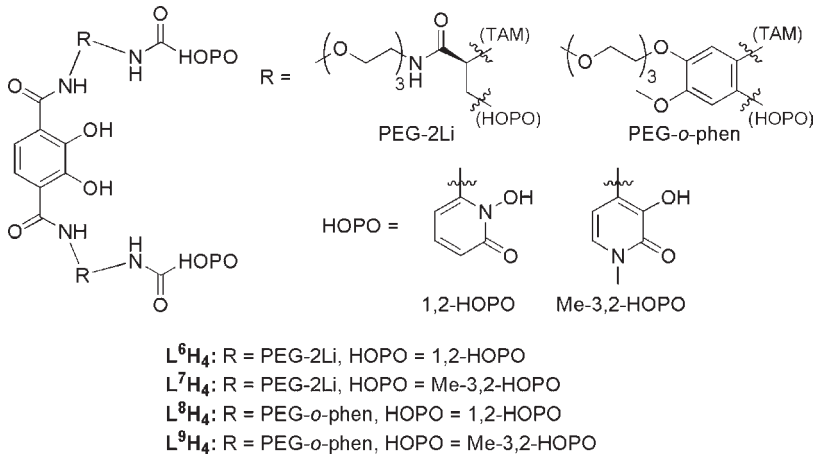

$\mathbf{L^6H_4}$: R = PEG-2Li, HOPO = 1,2-HOPO
$\mathbf{L^7H_4}$: R = PEG-2Li, HOPO = Me-3,2-HOPO
$\mathbf{L^8H_4}$: R = PEG-*o*-phen, HOPO = 1,2-HOPO
$\mathbf{L^9H_4}$: R = PEG-*o*-phen, HOPO = Me-3,2-HOPO

Figure 7. Water-soluble PEG-TAM$(HOPO)_2$ ligands.

by hexadentate TAM$(HOPO)_2$ ligands. Interplanar angles are calculated using the mean squared planes defined by the six ring atoms in the TAM and HOPO moieties and the six coordinating oxygen atoms from the TAM$(HOPO)_2$ ligands, respectively. Assuming that the unconstrained coordination geometry of a HOPO or TAM moiety is nearly coplanar with the uranyl coordination plane,[33] the ideal values for all the angles in Table 4 are 0°. The differences in interplanar angles necessarily result from a combination of twists through and bends out of the uranyl coordination plane by the chelating moieties, and thus vary significantly between $\{UO_2[TAM(HOPO)_2]\}^{2-}$ structures. One notable result is that $(\mathbf{L^2})^{4-}$ imposes the most planar orientation, with a maximum interplanar angle of 12.3° between the HOPO and TAM moieties; this value is only slightly larger than interplanar angles observed in tetradentate UO_2-(bis-Me-3,2-HOPO) complexes.[33] Ligands $(\mathbf{L^4})^{4-}$ and $(\mathbf{L^5})^{4-}$ generate interplanar angles between 5.1° and 81.8°, illustrating the steric consequences of the *o*-phenylene linker. Significantly, the range of interplanar angles observed in the *o*-phenylene-linked ligands supports our belief that the crystal structures in Figure 3 do not necessarily represent lowest energy conformations and that uranyl complexes with $(\mathbf{L^4})^{4-}$ and $(\mathbf{L^5})^{4-}$ in fact experience considerable flexibility in solution despite their rigid linkers. Such flexibility must therefore also be assumed in complexes with $(\mathbf{L^2})^{4-}$ due to the flexibility of the ethylene linker.

The variety in ligand conformation and bond distances observed in the $\{UO_2[TAM(HOPO)_2]\}^{2-}$ structures naturally introduces the question of which molecule most strongly binds the uranyl cation: The relatively long $U-O_{HOPO}$ bonds suggest that individual chelate strength may suffer in TAM$(HOPO)_2$ topologies compared to tetra- or bidentate ligands, but the increased chelate effect should yield high uranyl affinities.

Soluble Ligand Design. Aqueous thermodynamic measurements were performed to determine the uranyl affinity of TAM$(HOPO)_2$ ligands. However, more soluble TAM$(HOPO)_2$ ligands were needed for such measurements because while $\mathbf{L^1H_4}$, $\mathbf{L^2H_4}$, and $\mathbf{L^3H_4}$ were soluble enough for protonation constant measurements at 50 μM concentrations, $\mathbf{L^4H_4}$ and $\mathbf{L^5H_4}$ were too insoluble due to the *o*-phenylene linkers. Water solubility was introduced to TAM$(HOPO)_2$ ligands using the methyl-protected triethyleneglycol moiety (referred to hereon as PEG) on the linker moieties.

PEG group location in TAM$(HOPO)_2$ ligands was important because minimal electronic or steric influence was desirable in water-soluble ligands for consistency with their unsubstituted analogues. Substitution on the linker moieties was thus the only plausible location for the PEG moieties because they would be removed from the ligand coordination pocket and have the least possible affect on the electronic properties of the TAM and HOPO aromatic moieties. Some degree of inductive influence upon PEG substitution was unavoidable,[35] but structural and electronic influences are known to be mild in similar bis-Me-3,2-HOPO ligands. Four PEG-containing TAM$(HOPO)_2$ ligands were synthesized ($\mathbf{L^6H_4}$ through $\mathbf{L^9H_4}$, Figure 7), and all exhibit better aqueous solubility than $\mathbf{L^1H_4}$ through $\mathbf{L^5H_4}$ in both their neutral and deprotonated forms.

The uranyl affinities of TAM$(HOPO)_2$ ligands were expected to be significantly greater than those of bis-Me-3,2-HOPO moieties previously reported,[35] but to determine if denticity or TAM moiety inclusion is responsible for this effect, two tetradentate TAM-2Li-Me-3,2-HOPO ligands were designed, one with and one without a PEG moiety ($\mathbf{L^{10}H_3}$ and $\mathbf{L^{11}H_3}$, Figure 8). Ligands $\mathbf{L^{10}H_3}$ and $\mathbf{L^{11}H_3}$ present a tetradentate

dx.doi.org/10.1021/ja201511u |*J. Am. Chem. Soc.* 2011, 133, 7942–7956

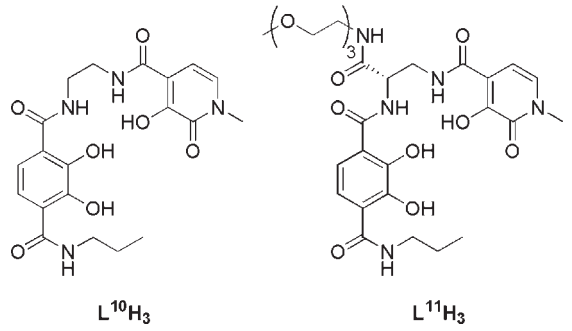

Figure 8. Tetradentate TAM-2Li-Me-3,2-HOPO ligands.

ligand geometry toward the uranyl cation similarly to bis-Me-3,2-HOPO ligands,[33−35] but the TAM moiety makes their electrostatic properties more similar to TAM(HOPO)$_2$ ligands. By comparing the uranyl affinities of $\mathbf{L^{10}H_3}$ and $\mathbf{L^{11}H_3}$ against those of tetradentate PEG-2Li-Me-3,2-HOPO[35] and hexadentate PEG-TAM(HOPO)$_2$ ligands, it can be determined whether increased TAM(HOPO)$_2$ uranyl affinity is caused by high denticity and chelate effect or solely by the inclusion of the TAM moiety.

Solution Thermodynamics. Because TAM and HOPO moieties require deprotonation for efficient metal chelation, their metal affinity is necessarily pH dependent. The most common pH in biological applications is that of blood serum (pH 7.4), but it is also desirable to investigate the uranyl affinity of polybidentate ligands in acidic and caustic media, as such conditions are encountered in industrial and waste remediation applications.[59,60] In the presence of dissolved metal ion (M^{a+}) and protonated ligand (LH_b, where L is ligand with b removable protons), the pH-dependent metal−ligand complex $M_mL_lH_h$ forms according to the equilibrium shown in Eq. 1. The relative amount of each species in solution is determined by Eq. 2, the rearrangement of which provides the standard formation constant notation of $\log \beta_{mlh}$ (Eq. 3). The $\log \beta_{mlh}$ value describes a cumulative formation constant, and a stepwise formation constant, $\log K$, can be calculated from $\log \beta_{mlh}$ values using Eq. 4. When addressing protonation constants, the stepwise formation constants are commonly reported as dissociation constants ($-\log K$, or pK_a), and are done so in this study.

$$mM^{a+} + lL^{b-} + hH^{+} \overset{\beta_{mlh}}{\rightleftharpoons} M_mL_lH_h^{(ma - lb + h)+} \quad \text{(Eq. 1)}$$

$$[M_mL_lH_h] = \beta_{mlh}[M]^m[L]^l[H]^h \quad \text{(Eq. 2)}$$

$$\log \beta_{mlh} = \log\left(\frac{[M_mL_lH_h]}{[M]^m[L]^l[H]^h}\right) \quad \text{(Eq. 3)}$$

$$\log K_{01n} = \log\left(\frac{[LH_n]}{[LH_{n-1}][H]}\right) = \log\left(\frac{\beta_{01n}}{\beta_{01(n-1)}}\right) = \log \beta_{01n} - \log \beta_{01(n-1)} \quad \text{(Eq. 4)}$$

Protonation constants were determined using spectrophotometric techniques at ligand concentrations of 4−6 μM with a starting DMSO concentration of ∼5%. Despite their PEG substituents, $\mathbf{L^8H_4}$ and $\mathbf{L^9H_4}$ were only sparingly soluble in neutral aqueous solution, so spectrophotometric titrations with these ligands were performed at 2 μM. Ligand titrations were typically performed between pH 3−11. Ligands containing the more acidic 1,2-HOPO moiety required measuring as low as pH 2.5, and some experiments needed to be brought as high as pH 11.5 because of the basic TAM phenols. Titrations were performed from acidic to basic pH, but subsequent return to acidic pH revealed poor reversibility which only worsened with increased equilibration time (see Supporting Information for reversibility plots). Irreversibility was presumably caused by the oxidation of the TAM moiety at very basic pH by trace oxygen in the titration cell; as a result, no reverse titrations (basic to acidic pH) were used in determining ligand protonation constants. The pK_a values determined by spectrophotometric titrations are listed in Table 5 along with the pK_a sums (ΣpK_a), which are an overall measure of ligand acidity; lower values indicate decreased proton affinity.

Table 5. pK_a Values for Tetra- and Hexadentate Ligands

ligand	pK_{a1}	pK_{a2}	pK_{a3}	pK_{a4}	ΣpK_a
$\mathbf{L^1H_4}$	4.91(3)	6.56(8)	8.7(1)	10.7(2)	30.9(2)
$\mathbf{L^2H_4}$	5.62(8)	6.65(8)	8.12(6)	11.16(9)	31.6(2)
$\mathbf{L^3H_4}$	4.94(1)	6.48(1)	8.44(3)	11.12(4)	30.98(5)
$\mathbf{L^6H_4}$	3.90(5)	5.53(3)	7.78(1)	9.95(1)	27.16(6)
$\mathbf{L^7H_4}$	4.5(1)	6.35(2)	9.22(2)	10.89(4)	30.96(5)
$\mathbf{L^8H_4}$	3.20(8)	5.10(7)	7.1(1)	9.8(2)	25.2(2)
$\mathbf{L^9H_4}$	4.7(1)	6.7(1)	7.13(9)	10.07(5)	28.6(2)
$\mathbf{L^{10}H_3}$	5.89(5)	6.8(1)	10.6(1)	–	23.3(2)
$\mathbf{L^{11}H_3}$	4.3(1)	6.15(5)	10.46(6)	–	20.9(1)

The first two protonation constants for TAM(HOPO)$_2$ ligands (pK_{a1} and pK_{a2}) and the first for $\mathbf{L^{10}H_3}$ and $\mathbf{L^{11}H_3}$ (pK_{a1}) correspond to deprotonation of the HOPO moieties,[35,36] while the last two protonation constants for both ligand types are those of the TAM moiety.[47] The 1,2-HOPO moieties in $\mathbf{L^1H_4}$, $\mathbf{L^6H_4}$, and $\mathbf{L^8H_4}$ are responsible for the depressed pK_{a1} and pK_{a2} values compared to their Me-3,2-HOPO-containing analogues $\mathbf{L^2H_4}$, $\mathbf{L^7H_4}$, and $\mathbf{L^9H_4}$, consistent with prior results.[36] Additionally, the presence of the PEG-amide group in $\mathbf{L^6H_4}$, $\mathbf{L^7H_4}$, and $\mathbf{L^{11}H_3}$ lowers each pK_a value compared against those of their unsubstituted analogues ($\mathbf{L^1H_4}$, $\mathbf{L^2H_4}$, and $\mathbf{L^{10}H_3}$). This effect has been observed in PEG-substituted bis-Me-3,2-HOPO ligands and is most likely caused by a hydrogen-bonding stabilization of the deprotonated phenol or *N*-hydroxide oxygens of the TAM and/or HOPO moieties.[35] This interaction, in turn, is enabled by the close proximity of the PEG-amide functionality to the HOPO and TAM moieties.

Another observable trend is that the *o*-phenylene linkers make $\mathbf{L^8H_4}$ and $\mathbf{L^9H_4}$ more acidic compared to their ethylenediamine-linked analogues $\mathbf{L^1H_4}$, $\mathbf{L^2H_4}$, $\mathbf{L^6H_4}$, and $\mathbf{L^7H_4}$. This can be attributed to the extended conjugation introduced by the *o*-phenylene linker, which may better stabilize negative charge buildup upon deprotonation. Because poor solubility prevents thermodynamic evaluation of $\mathbf{L^4H_4}$ and $\mathbf{L^5H_4}$, it is impossible to discern whether increased acidity is due to the extended ligand conjugation or alkoxy substitution.

The TAM deprotonation constants (pK_{a3} and pK_{a4}) in TAM-(HOPO)$_2$ ligands display an interesting trend when compared to the published monobidentate TAM pK_a values of 6.0−6.5 and 10.3−11.0.[47] Namely, while the second TAM proton in TAM-(HOPO)$_2$ ligands exhibits the expected high pK_a value of ∼11,

dx.doi.org/10.1021/ja201511u |*J. Am. Chem. Soc.* 2011, 133, 7942–7956

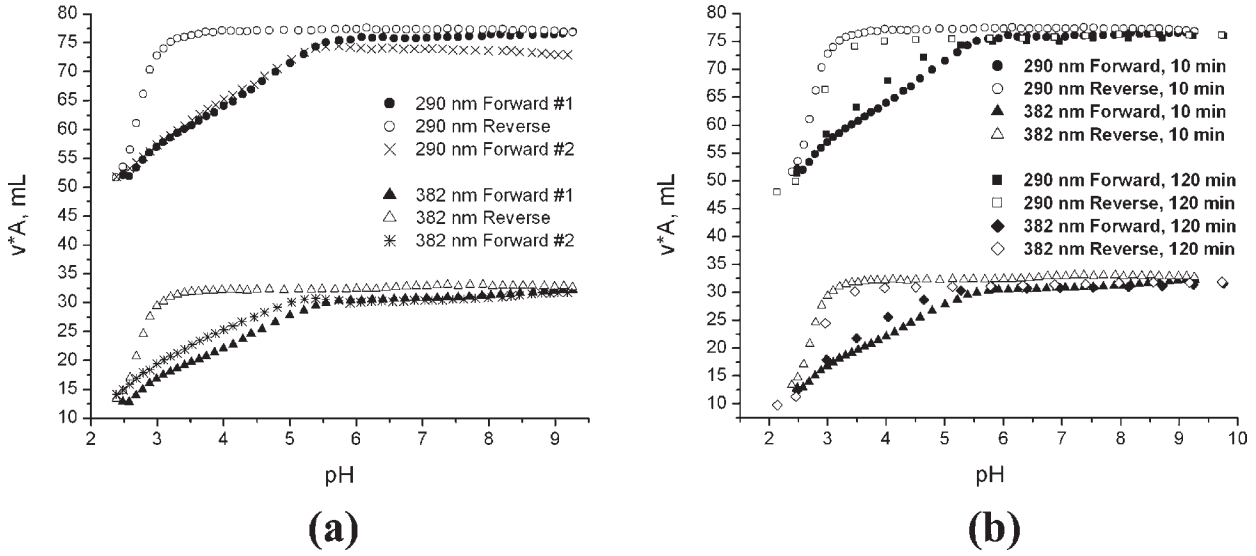

Figure 9. Spectrophotometric reversibility plots of uranyl titrations with $\mathbf{L^1H_4}$: (a) 10-min equilibration time illustrating lack of ligand/complex decomposition; (b) overlay of two separate, identical titrations illustrating hysteresis between 10- and 120-min equilibration times.

the first TAM proton has a pK_a between 1 and 3 orders of magnitude higher than expected. In contrast, both TAM pK_a values in tetradentate $\mathbf{L^{10}H_3}$ and $\mathbf{L^{11}H_3}$ are very close to those of monomeric TAM moieties. We hypothesize this discrepancy stems from the different position of the TAM moiety in the two ligand types: the terminal amide group in $\mathbf{L^{10}H_3}$ and $\mathbf{L^{11}H_3}$ can provide dedicated hydrogen-bond stabilization to only one phenolate oxygen, whereas the linking TAM amides in TAM-$(HOPO)_2$ ligands can provide stabilization to both a phenolate TAM oxygen as well as a *N*-hydroxide/phenolate oxygen on the HOPO moiety. Thus the TAM phenols in $\mathbf{L^{10}H_3}$ and $\mathbf{L^{11}H_3}$ are on average better stabilized upon deprotonation than those in TAM$(HOPO)_2$ ligands, lowering their pK_{a2} values compared to pK_{a3} in TAM$(HOPO)_2$ ligands.

Uranyl titrations were monitored spectrophotometrically using a 1:1 metal-to-ligand ratio to avoid decomposition of free ligand at high pH. It was assumed that maintaining this ratio would also ensure mononuclear complexes of the sort observed in crystallographic analysis. Ligand concentrations during these measurements ranged between 2−6 μM with a starting DMSO concentration of ∼5% to facilitate solvation of less soluble, neutral uranyl species during the course of the titration. Equilibration time between data points was found to be of great importance: uranyl titrations with ligands $\mathbf{L^1H_4}$, $\mathbf{L^2H_4}$, $\mathbf{L^3H_4}$, $\mathbf{L^6H_4}$, and $\mathbf{L^7H_4}$ using a 10-min equilibration time between data points displayed terrible reversibility which was found to be a kinetic effect and not caused by ligand or complex decomposition (Figure 9a). Extending equilibration time to 2 h revealed a kinetic hysteresis between pH 2.5 and 5.5 (Figure 9b). It was estimated that the equilibration time needed between pH 2.5 and 5.5 was at least 12−18 h, so batch titrations were performed with all TAM$(HOPO)_2$ ligands using 48−72-h equilibration times. In batch titrations $[UO_2^{2+}] = [L] = 1.3-2.0$ μM to accommodate for the 10-cm path length quartz-window UV/vis cell used. The extended equilibration times resulted in precipitation of either protonated ligand or neutral uranyl complexes at low pH when using $\mathbf{L^2H_4}$ and $\mathbf{L^3H_4}$ so that uranyl affinities could not be determined for these ligands. In contrast to the slow kinetics with TAM$(HOPO)_2$ ligands, uranyl titrations with tetradentate ligands $\mathbf{L^{10}H_3}$ and $\mathbf{L^{11}H_3}$ exhibited excellent reversibility with equilibration times of 10−20 min, and thus, titrations with these ligands were performed using incremental titrant addition methods with $[UO_2^{2+}] = [L] = 6$ μM and a 6.6 cm path length cell.

The uranyl titration spectra also reveal a significant difference between hexadentate and tetradentate complexes at high pH. Little change in the UV−visible spectra was observed above pH 8−9 with TAM$(HOPO)_2$ ligands regardless of equilibration time, suggesting that fully deprotonated, coordinatively saturated $\{UO_2[TAM(HOPO)_2]\}^{2-}$ complexes can form at relatively low pH and that no partial hydrolysis of the uranyl cation occurs upon increasing hydroxide concentration. In contrast, uranyl titrations with $\mathbf{L^{10}H_3}$ and $\mathbf{L^{11}H_3}$ exhibited dynamic spectroscopic behavior above pH 9, requiring titrations to be run as high as pH 11.4. Because the coordination modes of $\mathbf{L^{10}H_3}$ and $\mathbf{L^{11}H_3}$ are similar to that of bis-Me-3,2-HOPO ligands and do not saturate the uranyl coordination plane, it was expected that partial hydrolysis of the uranyl cation occurs at elevated pH, as it does with bis-Me-3,2-HOPO ligands.[33−35] Excellent reversibility at high pH indicated that the spectrum change was not due to ligand decomposition. Low pH titrations between pH 3.0 and 1.6 were also performed with $\mathbf{L^{10}H_3}$ and $\mathbf{L^{11}H_3}$ to help more fully characterize the complex formation.

One notable result was that $\mathbf{L^9H_4}$, like the other TAM-$(HOPO)_2$ ligands, inhibited hydrolysis of the uranyl cation at elevated pH. This was surprising because the structurally analogous $[UO_2(\mathbf{L^5})]^{2-}$ exhibited two very long U−O_{HOPO} bonds in Figure 3f, presumably due to ligand constraints. These weak U−O bonds were expected to yield to hydroxide coordination at high pH, but it seems that even these bonds successfully prevent uranyl hydrolysis at high pH. It is also possible that these bonds do not yield because the strained geometry in Figure 3f is only a solid-state effect and that in solution the average bond strength of the amide oxygens to the uranyl cation is greater than the crystal structure would suggest.

The difference in equilibration times, coupled with the deprotonation behavior of the tetra- and hexadentate uranyl complexes in this study suggest yet another important difference in uranyl complex formation stemming from ligand geometry: We

dx.doi.org/10.1021/ja201511u |*J. Am. Chem. Soc.* 2011, 133, 7942–7956

Scheme 1. Hypothesized Complexation Behavior of TAM(HOPO)$_2$ Ligands (L^1H_4 shown as example)[a]

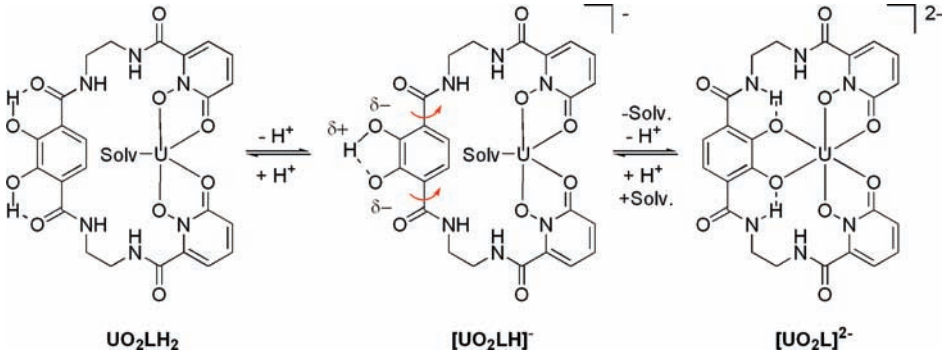

[a] Uranyl oxo atoms are omitted for clarity and hydrogen-bonding interactions are only indicated for the TAM moiety.

hypothesize that the kinetic barrier observed in uranyl titrations with TAM(HOPO)$_2$ ligands is associated with TAM moiety rotation upon complete deprotonation (Scheme 1). It is assumed that both HOPO moieties simultaneously deprotonate at low pH[35] to form a UO_2LH_2 complex in which only HOPO moieties chelate the uranium atom, with the uranyl coordination plane possibly completed by a coordinated solvent molecule. The protonated TAM moiety would most likely be oriented away from the uranyl cation and hydrogen bonded to the amide oxygen atoms as observed in protonated TAM species.[45,47,61] Upon increasing pH the TAM phenols sequentially deprotonate, forming first a $[UO_2LH]^-$ complex in which the hydrogen-bonding network is disrupted, and allowing slow rotation and displacement of coordinated solvent at the uranyl center by the TAM moiety. Upon full deprotonation and uranyl coordination to form a $[UO_2L]^{2-}$ complex, the TAM phenolates regain a favorable intramolecular hydrogen-bonding interaction with the ortho amide protons, explaining the kinetic barrier observed upon lowering pH and reversing the process. Following this reasoning, uranyl titration data with TAM(HOPO)$_2$ ligands were refined using UO_2LH_2, $[UO_2LH]^-$, and $[UO_2L]^{2-}$ species, assuming that the HOPO protons are of such similar pK_a values that they simultaneously deprotonate upon initial uranyl chelation.

In contrast to the slow kinetics observed in TAM(HOPO)$_2$ metalation titrations, the kinetic time scales observed with $\mathbf{L^{10}H_3}$ and $\mathbf{L^{11}H_3}$ were comparable to those with bis-Me-3,2-HOPO ligands,[35] suggesting that there is little to no kinetic barrier for tetradentate uranyl chelation. The relatively low value of one TAM pK_a in both of these ligands is comparable to the pK_a of Pr-Me-3,2-HOPO (pK_a = 6.12),[62] and because of its similarity to bis-Me-3,2-HOPO ligands, it is reasonable to suppose that initial uranyl chelation occurs via simultaneous and complete deprotonation of the HOPO and TAM moieties to generate an anionic $[UO_2L(solv.)]^-$ complex. Data refinement using more stepwise deprotonation was unstable and not supported by factor analysis. A partial hydrolysis of the uranyl center occurs upon increasing pH, resulting in a $[UO_2L(OH)]^{2-}$ species, consistent with other tetradentate ligands that inadequately saturate the uranyl coordination plane (Scheme 2).[35,63]

The uranyl formation constants (log β_{mlh}) for the TAM-(HOPO)$_2$ and TAM-2Li-Me-3,2-HOPO ligands are reported in Table 6. Because log β_{mlh} values are species dependent, a species-independent metric is needed to compare uranyl affinities of the bis- and tris-bidentate ligands studied here. The metric employed

Scheme 2. Proposed Speciation in Uranyl Titrations with TAM-2Li-Me-3,2-HOPO Ligands ($L^{10}H_3$ shown as example)[a]

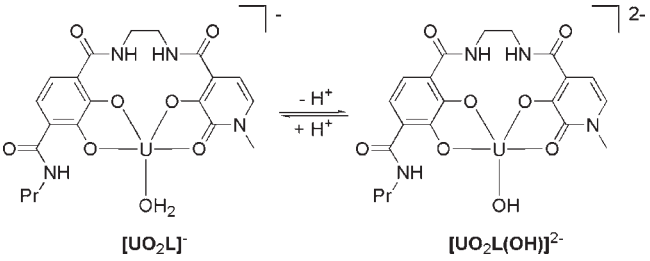

[a] Uranyl oxo atoms are omitted for clarity.

Table 6. Log β_{mlh} and pUO$_2$ Values for TAM-Containing Ligands

					pUO$_2$[a]		
ligand	log β_{11-1}	log β_{110}	log β_{111}	log β_{112}	pH 3.0	pH 7.4	pH 9.0
L^1H_4	—	21.95(4)	26.86(8)	30.79(2)	6.9(3)	18.2(3)	21.0(3)
L^6H_4	—	17.9(3)	24.8(2)	29.4(2)	9.2(3)	15.9(3)	17.8(3)
L^7H_4	—	21.5(5)	28.7(4)	32.0(4)	8.1(5)	17.3(5)	20.1(6)
L^8H_4	—	19.1(6)	25.0(4)	30.0(3)	11.5(4)	17.5(8)	19.2(8)
L^9H_4	—	19.0(5)	25.7(2)	29.5(4)	7.9(5)	17.1(5)	18.8(6)
$L^{10}H_3$	11.92(6)	19.75(1)	—	—	6.6(1)	17.5(1)	20.3(2)
$L^{11}H_3$	10.31(9)	17.9(1)	—	—	7.0(2)	16.0(2)	18.8(1)

[a] pUO$_2$ = $-\log[UO_2^{2+}{}_{free}]$; $[UO_2^{2+}] = 10^{-6}$ M and $[L] = 10^{-5}$ M

for that purpose is pUO$_2$, where pUO$_2$ = $-\log[UO_2^{2+}{}_{free}]$. "$UO_2^{2+}{}_{free}$" refers to solvated uranyl ion free of complexation by ligand or hydroxide, with a higher pUO$_2$ corresponding to a lower concentration of uncomplexed uranyl in solution. As a pertinent benchmark, pUO$_2$ in oceanic conditions is 16.8 due to the high affinity of carbonate for the uranyl cation.[25,64] pUO$_2$ values in this study are calculated using standard conditions of $[UO_2^{2+}] = 10^{-6}$ M and $[L] = 10^{-5}$ M (L:M = 10), and thus the minimum pUO$_2$ value of 6.0 corresponds to completely uncomplexed uranyl cation. While typically reported at physiological pH, pUO$_2$ can be calculated at any pH upon determination of pK_a and log β_{mlh} values; pUO$_2$ values at pH 3.0, 7.4, and 9.0 are listed for each ligand in Table 6. The relatively large errors in

dx.doi.org/10.1021/ja201511u |J. Am. Chem. Soc. 2011, 133, 7942–7956

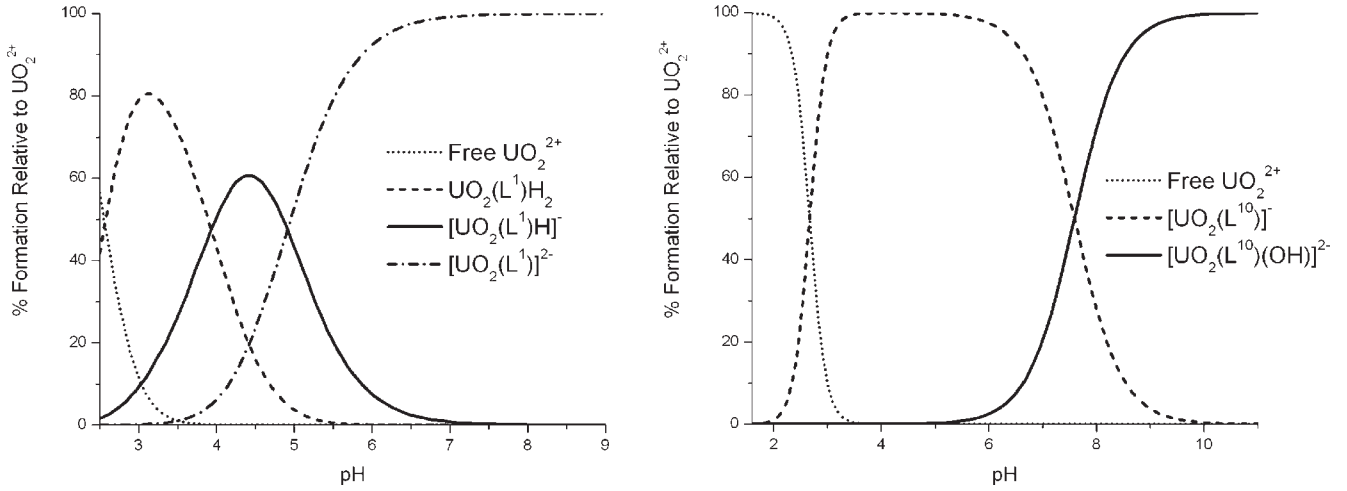

Figure 10. Representative speciation diagrams for uranyl complexes with TAM(HOPO)$_2$ ($\mathbf{L^1H_4}$, left) and TAM-2Li-Me-3,2-HOPO ($\mathbf{L^{10}H_3}$, right) ligands at standard pUO_2 conditions ($[UO_2^{2+}] = 10^{-6}$ M, [L] = 10^{-5} M).

pUO_2 values result from a combination of the ~0.1−0.2 error in ligand pK_a values and the ~0.1−0.6 error in log β_{mlh} values, which are themselves a consequence of the low concentrations and large volumes required in the uranyl titrations to achieve aqueous solubility and allow UV−visible measurements in long path length cells, respectively.

Representative speciation diagrams of the uranyl complexes with TAM(HOPO)$_2$ and TAM-2Li-Me-3,2-HOPO ligands are illustrated in Figure 10; comprehensive speciation diagrams and UV−visible titration spectra of all ligands are provided in the Supporting Information. Notably, initial uranyl chelation by TAM(HOPO)$_2$ ligands $\mathbf{L^1H_4}$ through $\mathbf{L^9H_4}$ is complete below pH 2.5, while for TAM-2Li-Me-3,2-HOPO ligands $\mathbf{L^{10}H_3}$ and $\mathbf{L^{11}H_3}$ this is still incomplete at pH 3. We hypothesize this difference exists because initial complex formation with TAM-(HOPO)$_2$ ligands requires deprotonation only of the acidic HOPO moieties, while complexation by TAM-2Li-Me-3,2-HOPO ligands also requires deprotonation of the more basic TAM moiety. In fact, the complete deprotonation of the TAM moiety in $\mathbf{L^{10}H_3}$ and $\mathbf{L^{11}H_3}$ represents an effective maximum pK_a shift of ~8 log units in the presence of the uranyl cation as compared to the free ligand. This illustrates the strong inductive effect of the uranyl cation that is known to cause effective pK_a shifts as high as 13 orders of magnitude in chelating ligands.[65] Such an extreme inductive effect on TAM moiety pK_a is not observed with TAM(HOPO)$_2$ ligands because of the geometric consequences discussed above.

The pUO_2 values of both tetra- and hexadentate ligands are significantly higher than those of bis-Me-3,2-HOPO ligands at all pH values.[35] This was expected for the TAM(HOPO)$_2$ ligands due to their higher denticity. However, the pUO_2 values of the tetradentate TAM-2Li-Me-3,2-HOPO ligands reveal the TAM moiety to have a very strong effect on pUO_2, which is necessarily a significant influence in the hexadentate ligands as well. This general result is consistent with the known strong affinity of TAM moiety toward hard Lewis acids such as Fe(III).[47] It is important to note that any increase in pUO_2 upon increasing pH is partially due to ligand-independent reduction of $[UO_2^{2+}{}_{free}]$ caused by increased uranyl hydrolysis. Because speciation diagrams of uranyl with TAM(HOPO)$_2$ ligands indicate formation of a $[UO_2(L)]^{2-}$ complex by pH 8, we hypothesize the increase in pUO_2 of 2 to 3 log units between pH 7.4 and pH 9.0 is primarily caused by hydrolysis of free uranyl ion. In contrast, the rise in pUO_2 (typically 6 to 10 log units) between pH 3.0 and pH 7.4 is primarily caused by increased uranyl affinity due to TAM deprotonation which increases chelate strength. Increased pUO_2 of TAM-2Li-Me-3,2-HOPO ligands upon increasing pH can be explained in a similar manner. In particular, it should be noted that although hydrolysis of the uranyl cation occurs at elevated pH with $\mathbf{L^{10}H_3}$ and $\mathbf{L^{11}H_3}$, this does not significantly influence ligand affinity, and the increase in pUO_2 between pH 7.4 and pH 9.0 is again primarily caused by an increase in hydrolysis of free uranyl cation.

The pUO_2 values of most TAM(HOPO)$_2$ ligands at pH 7.4 and 9.0 are within experimental error of each other, so the effect of subtle changes in ligand geometry are unfortunately indiscernible from this study. It was expected that the *o*-phenylene backbone in $\mathbf{L^8H_4}$ and $\mathbf{L^9H_4}$ would at the very least cause a measurable difference in pUO_2 compared to $\mathbf{L^6H_4}$ and $\mathbf{L^7H_4}$ because of the significant geometric variations observed in the structures of their respective uranyl complexes. However, the differences in pUO_2 values are below the error associated with the batch titration methods. In contrast, pUO_2 values at pH 3.0 do show significant variation between TAM(HOPO)$_2$ ligands. As mentioned above, the TAM moiety does not coordinate the uranyl cation at low pH, leaving only the HOPO moieties available to bind the uranyl cation. In support of this theory, higher pUO_2 values at pH 3.0 are observed in ligands incorporating the more acidic 1,2-HOPO moiety ($\mathbf{L^6H_4}$ versus $\mathbf{L^7H_4}$; $\mathbf{L^8H_4}$ versus $\mathbf{L^9H_4}$). Ligand $\mathbf{L^8H_4}$ demonstrated the highest pUO_2 at pH 3 due to a combination of the intrinsically low pK_a of 1,2-HOPO moieties coupled with the tendency for the PEG-substituted *o*-phenylene linkers to lower the pK_a of their associated ligand moieties.[35]

The pUO_2 of ligands $\mathbf{L^{10}H_3}$ and $\mathbf{L^{11}H_3}$ at pH 3.0 are generally lower than those of TAM(HOPO)$_2$ ligands and similar to those of tetradentate bis-Me-3,2-HOPO ligands.[35] These relatively low pUO_2 values result from the need of $\mathbf{L^{10}H_4}$ and $\mathbf{L^{11}H_3}$ to lose three protons to achieve initial uranyl chelation, while TAM-(HOPO)$_2$ ligands need only lose their two most acidic HOPO protons. In contrast, the pUO_2 values of $\mathbf{L^{10}H_3}$ and $\mathbf{L^{11}H_3}$ are surprisingly similar at physiological and basic pH to those of

dx.doi.org/10.1021/ja201511u |*J. Am. Chem. Soc.* 2011, 133, 7942–7956

$TAM(HOPO)_2$ ligands, suggesting that the most influential chelating moiety in these ligands is the TAM moiety. Namely, bis- and tris-bidentate ligands are not expected to exhibit similar metal affinities assuming that all possible coordinating atoms are capable of simultaneous metal coordination. However, the high pUO_2 values of $\mathbf{L^{10}H_3}$ and $\mathbf{L^{11}H_3}$ reveal that the change in geometry from tetradentate to hexadentate is not as significant as the inclusion of the more basic and strongly binding TAM moiety into the ligand scaffold. This conclusion is supported by the crystallographic studies of $\{UO_2[TAM(HOPO)_2]\}^{2-}$ complexes, which revealed an invariance in the $U-O_{TAM}$ distance despite linker and HOPO moiety variation.

CONCLUSIONS

Coordinative saturation of the uranyl cation has been achieved by the development of hexadentate $TAM(HOPO)_2$ ligands utilizing short alkyl and aromatic linkers. Hexadentate chelation is accompanied by a variety of molecular distortions, throughout which the TAM moiety maintains the shortest and most consistent equatorial U−O bond distances. The dominance of the TAM moiety in uranyl binding is supported by solution phase thermodynamic measurements with TAM-2Li-Me-3,2-HOPO ligands, which have remarkably high pUO_2 values despite their lower denticity. Unfortunately, uranyl affinities of the investigated ligands were within experimental error at physiological and basic pH, obscuring the effect of minor geometric differences between ligands.

Future ligand design strategies for selective actinyl complexation are informed by several of the results reported here. First, the speciation of UO_2[TAM-2Li-Me-3,2-HOPO] complexes supports the known phenomenon that basic chelating moieties are capable of undergoing complete deprotonation at low pH if coupled to an acidic chelating moiety that simultaneously binds the metal cation.[65] Second, the spatial arrangement of binding moieties of differing pK_a can result in undesirably slow binding kinetics, especially in cations with well-defined coordination modes. A method to avoid the slow binding kinetics of $TAM(HOPO)_2$ ligands would be to put the most basic moiety at the terminal position of a linear, polybidentate ligand. This arrangement may utilize the best traits of both the $TAM(HOPO)_2$ and TAM-2Li-Me-3,2-HOPO ligands without their respective drawbacks. Namely, the increased denticity and TAM inclusion would enhance pUO_2, but would also impart flexibility to the TAM moiety such that it could bind in concert with the lower-acidity chelating moieties. This geometric property should in turn depress the effective pK_a of the TAM moiety and allow high efficiency chelation at low pH.

The substitution strategies used to solubilize the ligands in this study could similarly be employed as tethers to a variety of larger molecules or solid supports for various extraction or sensing applications. Although substitution on the linker moieties does affect ligand pK_a, the influence on uranyl affinity is small, leaving the efficacy of these ligand platforms largely preserved. Finally, a conclusion taken from the asymmetric location of the uranyl cation within the $TAM(HOPO)_2$ binding pocket is that this ligand system may be more applicable toward actinyl cations of larger radii, such as UO_2^+ and NpO_2^+, in which ligand distortions may be lessened and M-O bond equality could be better realized.

EXPERIMENTAL SECTION

General. All reactions brought to reflux were done so with an efficient condenser attached to the reaction flask. NMR spectra were collected using Bruker AMX-400 and AM-400 spectrometers (^{1}H 400 MHz, ^{13}C 100 MHz) in DMSO-d_6. Mass spectrometry and elemental analyses were performed at the Microanalytical Facility, College of Chemistry, University of California, Berkeley. Yields indicate the amount of isolated compound, and reactions are unoptimized.

UO_2(*o*-phen-1,2-HOPO), UO_2(phen12HP). A solution of *o*-phen-1,2-HOPO[50] (31 mg, 0.081 mmol) and 3 drops of pyridine were dissolved in 15 mL of MeOH, and a solution of $UO_2(NO_3)_2\cdot 6H_2O$ (37 mg, 0.074 mmol) in 2 mL of MeOH was added. The mixture was stirred at reflux overnight. After cooling to room temperature, the precipitate was filtered, washed with MeOH, and dried under vacuum to yield 40 mg of an orange solid, 83%. Anal. Calcd (Found) for $C_{18}H_{12}N_4O_8U$: C, 33.24 (33.19); H, 1.86 (1.90); N, 8.62 (8.47). ^{1}H NMR: δ 7.33 (dd, ^3J(H,H) = 6.4, 3.6 Hz, 2H; HOPO H), 7.38 (dd, ^3J(H,H) = 8.4, 1.6 Hz, 2H; arom. H), 7.73, (dd, ^3J(H,H) = 7.6, 1.6 Hz, 2H; arom. H), 7.96 (t, ^3J(H,H) = 8.0 Hz, 2H; HOPO H), 8.48 (dd, ^3J(H,H) = 6.4, 3.6 Hz, 2H; HOPO H), 12.51 (s, 2H; NH). ^{13}C NMR: δ 115.46, 118.74, 123.48, 125.15, 128.45, 136.75, 139.13, 157.66, 163.63. MS (FAB^+): m/z 651 (MH^+).

UO_2[TAM(2Li-Me-3,2-HOPO)$_2$]·2(NMe_4), $UO_2(L^2)\cdot 2(NMe_4)$. A solution of $\mathbf{L^2H_4\cdot MeOH}$ (101 mg, 0.164 mmol) and $NMe_4OH\cdot 5H_2O$ (120 mg, 0.662 mmol) in 5 mL of MeOH was added to a stirred solution of 82.4 mg (0.164 mmol) of $UO_2(NO_3)_2\cdot 6H_2O$ in 2 mL MeOH. The dark-red solution was heated at reflux overnight, and the volume was reduced to 3 mL. Insoluble material was removed by filtering through glass wool, and the solution was layered with acetone to yield 106 mg of dark-red crystals which were filtered and dried by aspiration. These crystals were used for NMR and X-ray crystallographic analysis and were shown to be $UO_2(L^2)\cdot 2NMe_4\cdot Me_2CO$, 58%. Anal. Calcd (Found) for $C_{26}H_{24}N_6O_{12}U\cdot 2N(CH_3)_4\cdot 2C_3H_6O$ (%): C, 43.09 (42.87); H, 5.42 (5.33); N, 10.05 (10.00). ^{1}H NMR: δ 2.08 (s, 6H; CH_3), 3.05 (s, 24H; CH_3), 3.36 (s, 8H; OH_2), 3.59−3.63 (m, 8H; CH_2), 3.73 (s, 6H; CH_3), 6.81 (d, ^3J(H,H) = 7.2 Hz, 2H; HOPO H), 6.90 (d, ^3J(H,H) = 7.2 Hz, 2H; HOPO H), 6.92 (s, 2H; TAM H), 11.55 (t, ^3J(H,H) = 5.2 Hz, 2H; NH), 11.75 (t, ^3J(H,H) = 5.2 Hz, 2H; NH). ^{13}C NMR: δ 30.74, 36.46, 38.79, 54.30, 54.34, 54.38, 107.11, 113.34, 116.01, 117.30, 120.84, 161.80, 165.51, 166.90, 167.04, 167.49.

UO_2[TAM(*o*-phen-1,2-HOPO)$_2$]·2NMe_4, $UO_2(L^4)\cdot 2NMe_4$. A solution of $\mathbf{L^4H_4\cdot 1/2H_2O\cdot 1/2CH_3OH}$ (50 mg, 0.074 mmol) and $NMe_4(OH)\cdot 5H_2O$ (54 mg, 0.298 mmol) in 4 mL of MeOH was added to a stirred solution of $UO_2(NO_3)_2\cdot 6H_2O$ (37 mg, 0.074 mmol) in 1 mL of MeOH. The deep-red solution was heated at reflux overnight and cooled to room temperature, and the solvent was removed under vacuum. The residue was dissolved in 0.5 mL of DMSO, and THF was diffused into the solution at room temperature. Initial precipitates were generally colorless, so the crystallization solution was filtered every week to remove what was suspected to be NMe_4NO_3. Once dark material began to precipitate, the solution was filtered one last time and allowed to continue to diffuse at 4 °C. The crop of dark crystals and amorphous material was filtered, washed with THF, and allowed to dry by aspiration for 2 days, yielding 37 mg of crystalline and amorphous, dark solid that elemental and NMR analyses indicated was $UO_2(L^4)\cdot 2NMe_4\cdot DMSO\cdot H_2O\cdot 1/5THF\cdot 1/3NMe_4NO_3$. Anal. Calcd (Found) for $C_{32}H_{20}N_4O_{12}\cdot 2N(CH_3)_4\cdot C_2H_6OS\cdot H_2O\cdot 1/5C_4H_8O\cdot 1/3N(CH_3)_4NO_3$ (%): C, 43.35 (43.49); H, 4.75 (4.45); N, 9.93 (9.59); S, 2.62 (2.67). ^{1}H NMR: δ 1.74−1.77 (m, 0.9H; THF H), 2.54 (s, 6H; DMSO CH_3), 3.04 (s, 29H; CH_3), 3.58−3.61 (m, 0.9H; THF H), 7.11−7.22 (m, 8H; TAM H + HOPO H + arom. H), 7.55 (d, ^3J(H,H) = 6.8 Hz, 2H; HOPO H), 7.72 (t, ^3J(H,H) = 8.0 Hz, 2H; HOPO H), 8.43 (d, ^3J(H,H) = 8.4 Hz, 2H; arom. H), 8.67 (d, ^3J(H,H) = 8.4 Hz, 2H;

arom. H), 13.05 (s, 2H; NH), 14.16 (s, 2H; NH). ^{13}C NMR: δ 25.13, 40.42, 54.30, 54.34, 54.38, 67.03, 111.60, 114.33, 117.95, 122.01, 122.36, 122.51, 124.46, 126.85, 130.69, 133.45, 138.10, 158.18, 162.78, 166.49, 166.57. (MS (ESI$^-$): 459.1 (M^{2-}). X-ray-quality crystals could also be grown by layering a similarly prepared crude DMSO solution of the complex and accompanying salts with dioxane. After diffusion at room temperature, these aliquots yielded three X-ray-quality crystals reported above. These other crystals were grown from crude materials, and the mixtures of precipitates from which they were isolated were not suitable for NMR or elemental analysis measurements.

UO_2[TAM(*o*-phen-Me-3,2-HOPO)$_2$]·2NMe$_4$, UO_2(L^5)·2NMe$_4$. A solution of $\mathbf{L^5H_4}$·1/2H_2O·1/2HCl (100 mg, 0.141 mmol) and NMe_4(OH)·5H_2O (106 mg, 0.585 mmol) in 10 mL of MeOH was added to a stirred solution of $UO_2(NO_3)_2$·6H_2O (73.6 mg, 0.147 mmol) in 5 mL of MeOH. The resultant red suspension was stirred at reflux overnight, then cooled to room temperature and filtered. The solid was dried under vacuum, yielding 132 mg of brown powder isolated as the methanolic hydrate, 78%. Anal. Calcd (Found) for $C_{34}H_{24}N_6O_{12}U$·2[$N(CH_3)_4$]·CH_3OH·H_2O (%): C, 44.41 (44.40); H, 4.85 (4.56); N, 9.64 (9.44). Crystals of this complex were formed by diffusion of MeOH into a DMSO complex solution. X-ray crystallography revealed the crystals to be of the composition UO_2-[TAM(**3**−**5**)$_2$]·2NMe_4·2MeOH. NMR analysis was performed on these crystals. ^{1}H NMR: δ 3.02 (s, 24H; CH_3), 3.18 (d, ^3J(H,H) = 4.8 Hz, 6H; CH_3OH), 3.77 (s, 6H; CH_3), 4.10 (q, ^3J(H,H) = 4.8 Hz, 2H; CH_3OH), 6.97 (q, ^3J(H,H) = 7.2 Hz, 4H; arom. H), 7.07−7.18 (m, 6H; arom. H + TAM H), 12.89 (s, 2H; NH), 13.24 (s, 2H; NH). ^{13}C NMR: δ 36.65, 48.61, 54.28, 54.32, 54.36, 106.94, 114.13, 115.98, 117.43, 121.54, 121.72, 122.04, 122.94, 123.43, 127.84, 130.52, 161.29, 164.31, 166.38, 166.59. MS (ESI$^-$): m/z 473.1 (M^{2-}).

X-ray Diffraction Data Collection. Uranyl complex crystals were mounted on captan loops with oil and cooled under a controlled temperature stream of liquid nitrogen boil-off during data collection. X-ray diffraction data were collected using either Bruker SMART 1000 or APEX I detectors with Mo Kα radiation at the UC Berkeley X-ray crystallographic facility. All data were integrated by the program SAINT.[66,67] The data were corrected for Lorentz and polarization effects. Data were analyzed for agreement and possible absorption using XPREP, and an empirical absorption correction was applied in SADABS.[68,69] Equivalent reflections were merged without an applied decay correction. All structures were solved using direct methods and were expanded with Fourier techniques using the SHELXL package.[70] Least squares refinement of F^2 against all reflections was carried out to convergence with $R[I > 2\sigma(I)]$. Least squares planes and angles between them were calculated using the SHELXL package.[70] Further details on the crystallographic refinement of the crystal structures are provided in the Supporting Information.

Titration Solutions and Equipment. Corning high performance combination glass electrodes (response to [H^+] was calibrated before each titration[71]) were used together with either an Accumet pH meter or a Metrohm Titrino to measure the pH of the experimental solutions. Metrohm autoburets (Dosimat or Titrino) were used for incremental additions of acid or base standard solution to the titration cell. The titration instruments were fully automated and controlled using LabVIEW software.[72] Titrations were performed in 0.1 M KCl supporting electrolyte under positive Ar gas pressure. The temperature of the experimental solution was maintained at 25 °C by an externally circulating water bath. UV−visible spectra for incremental titrations were recorded on a Hewlett-Packard 8452a spectrophotometer (diode array), while those for batch titrations were recorded on a Cary 300 Scan UV−vis spectrophotometer using customized quartz-windowed cells. Solid reagents were weighed on a Metrohm analytical balance accurate to 0.01 mg. All titration solutions were prepared using distilled water that was purified by passing through a Millipore Milli-Q reverse osmosis cartridge system and degassed by boiling for 1 h while being purged under Ar. Carbonate-free 0.1 M KOH was prepared from Baker Dilut-It concentrate and was standardized by titrating against potassium hydrogen phthalate using phenolphthalein as an indicator. Solutions of 0.1 M HCl were similarly prepared and were standardized by titrating against sodium tetraborate decahydrate to Methyl Red end point.

Spectrophotometric Titration Methods. Ligand stock solutions were made by dissolving a weighed amount of ligand accurate to 0.01 mg in DMSO in a volumetric flask. These stock solutions were frozen when not in use to prevent ligand decomposition. A stock uranyl solution in 1.2 wt % nitric acid was purchased from Aldrich (4.22 mM) and used as received. All titrations were performed with a ∼5% starting concentration of DMSO added to the KCl solution to promote the solvation of protonated ligands and their neutral uranyl complexes. Spectrophotometric titrations were carried out in the presence of 10−20 equiv (as compared to ligand concentration) of NH_4Cl, MES, and HEPES buffers in order to dampen the pH change between incremental additions of titrant. Each addition of acid or base was followed by an equilibration period before pH and absorbance data were collected: 600 s for free ligand and 600−1200 s for titrations in the presence of UO_2^{2+}. Low-concentration batch titrations were allowed to equilibrate for three days with constant agitation before the pH was measured on a freshly calibrated electrode and the spectra were recorded. Spectra were recorded between 250−550 nm; The UV−visible silent region above ∼420 nm was monitored for baseline drift as an indication of precipitated material.

Ligand concentrations for spectrophotometric titrations with a 6.6 cm path length cell and incremental addition of titrant were approximately 2−6 μM. Ligand concentrations for batch titrations using a 10 cm path length cell were 1.3−2 μM. All uranyl titrations were conducted with a 1:1 ligand:metal ratio to avoid decomposition of metal-free TAM ligands at high pH. Metal-to-ligand ratios were controlled by careful addition of a ligand solution of known concentration in DMSO and a standardized uranyl solution in 1.2 wt % nitric acid to the titration apparatus. All titrations (including long-equilibration time batch titrations) were repeated a minimum of three times. Each titration involving incremental addition of titrant was run forward and backward (from acid to base and reverse) when the titrations were deemed reversible. Titrations with TAM(HOPO)$_2$ ligands were only performed down to pH 2.4, while those with tetradentate TAM-2Li-Me-3,2-HOPO ligands were performed down to pH 1.6 by performing two strong acid titrations between pH 3.0 and 1.6. Data from these titrations were combined with those from higher pH titrations to yield the reported values.

Titration Data Treatment. Spectrophotometric titration data were analyzed using the program pHab,[73] utilizing nonlinear least-squares regression to determine formation constants. Values for the hydrolysis product of the uranyl cation were taken from a recent literature publication.[74] Wavelengths between 250−400 nm were typically used for data refinement, although batch titration data was often truncated to ∼270−400 nm due to large errors in the data at the lower wavelengths that typically had much stronger absorbance that the rest of the spectrum. The number of absorbing species to be refined upon was determined by factor analysis within the pHab program suite.[73] Reversibility of the titrations was determined by comparison of the species- and concentration-independent value $A^*\nu$ (absorbance*volume) at selected wavelengths for the forward and reverse titrations. Speciation diagrams were generated using HYSS[75,76] titration simulation software and the protonation and metal complex formation constants determined by potentiometric and spectrophotometric titration experiments.

■ ASSOCIATED CONTENT

Supporting Information. Ligand design and synthesis details, crystallographic figures and refinement details, crystallographic

information files (CIF), titration data, and figures. This material is available free of charge via the Internet at http://pubs.acs.org.

AUTHOR INFORMATION

Corresponding Author
raymond@socrates.berkeley.edu

ACKNOWLEDGMENT

We thank Drs. Rebecca Abergel and Trisha Hoette for assistance with the titration measurements and data treatment. This research is supported by the Director, Office of Science, Office of Basic Energy Sciences, and the Division of Chemical Sciences, Geosciences, and Biosciences of the U.S. Department of Energy at LBNL under Contract No. DE-AC02-05CH11231.

REFERENCES

(1) This paper is #64 in the series "Specific Sequestering Agents for the Actinides." For the previous paper, see Ni, Chengbao; Shuh, D. K.; Raymond, K. N. *Chem. Commun.* DOI: 10.1039/c1cc11329a.
(2) Ansoborlo, É.; Amekraz, B.; Moulin, C.; Moulin, V.; Taran, F.; Bailly, T.; Burgada, R.; Hengé-Napoli, M.-H.; Jeanson, A.; Den Auwer, C.; Bonin, L.; Moisy, P. *C. R. Chim.* **2007**, *10*, 1010–1019.
(3) Gorden, A. E. V.; Xu, J.; Raymond, K. N. *Chem. Rev.* **2003**, *103*, 4207–4282.
(4) Maynadié, J.; Berthet, J.-C.; Thuery, P.; Ephritikhine, M. *Chem. Commun.* **2007**, 486–488.
(5) Berthet, J.-C.; Thuery, P.; Dognon, J.-P.; Guillaneux, D.; Ephritikhine, M. *Inorg. Chem.* **2008**, *47*, 6850–6862.
(6) Sarsfield, M. J.; Helliwell, M. *J. Am. Chem. Soc.* **2004**, *126*, 1036–1037.
(7) Wilkerson, M. P.; Burns, C. J.; Morris, D. E.; Paine, R. T.; Scott, B. L. *Inorg. Chem.* **2002**, *41*, 3110–3120.
(8) Sessler, J. L.; Seidel, D.; Vivian, A. E.; Lynch, V.; Scott, B. L.; Keogh, D. W. *Angew. Chem., Int. Ed.* **2001**, *40*, 591–594.
(9) Thuéry, P.; Masci, B.; Takimoto, M.; Yamato, T. *Inorg. Chem. Commun.* **2007**, *10*, 795–799.
(10) Zhang, W.; Zhao, J. *Inorg. Chem. Commun.* **2006**, *9*, 397–399.
(11) Masci, B.; Thuéry, P. *CrystEngComm.* **2007**, *9*, 582–590.
(12) Sarsfield, M. J.; Helliwell, M.; Raftery, J. *Inorg. Chem.* **2004**, *43*, 3170–3179.
(13) Burns, C. J.; Clark, D. L.; Donohoe, R. J.; Duval, P. B.; Scott, B. L.; Tait, C. D. *Inorg. Chem.* **2000**, *39*, 5464–5468.
(14) Danis, J. A.; Lin, M. R.; Scott, B. L.; Eichhorn, B. W.; Runde, W. H. *Inorg. Chem.* **2001**, *40*, 3389–3394.
(15) Thuéry, P.; Masci, B. *J. Chem. Soc., Dalton Trans.* **2003**, 2411–2417.
(16) Arnold, P. L.; Blake, A. J.; Wilson, C.; Love, J. B. *Inorg. Chem.* **2004**, *43*, 8206–8208.
(17) Arnold, P. L.; Patel, D.; Blake, A. J.; Wilson, C.; Love, J. B. *J. Am. Chem. Soc.* **2006**, *128*, 9610–9611.
(18) Franczyk, T. S.; Czerwinski, K. R.; Raymond, K. N. *J. Am. Chem. Soc.* **1992**, *114*, 8138–8146.
(19) Sather, A. C.; Berryman, O. B.; Rebek, J., Jr. *J. Am. Chem. Soc.* **2010**, *132*, 13572–13674.
(20) Copping, R.; Gaunt, A. J.; May, I.; Sharrad, C. A.; Collison, D.; Helliwell, M.; Fox, O. D.; Jones, C. J. *Chem. Commun.* **2006**, *36*, 3788–3790.
(21) Nocton, G.; Horeglad, P.; Pécaut, J.; Mazzanati, M. *J. Am. Chem. Soc.* **2008**, *130*, 16633–16645.
(22) Madic, C.; Begun, G. M.; Hobart, D. E.; Hahn, L. *Radiochim. Acta* **1983**, *34*, 195–202.
(23) Walton, P. H.; Raymond, K. N. *Inorg. Chim. Acta* **1995**, *240*, 593–601.
(24) Beer, S.; Berryman, O. B.; Ajami, D.; Rebek, J., Jr. *Chem. Sci.* **2010**, *1*, 43–47.
(25) Schwochau, K. *Top. Curr. Chem.* **1984**, *124*, 91–133.
(26) Alexander, V. *Chem. Rev.* **1995**, *95*, 273–342.
(27) Fenton, D. E.; Vigato, P. A. *Chem. Soc. Rev.* **1988**, *17*, 69–90.
(28) Dam, H. H.; Reinhoudt, D. N.; Verboom, W. *Chem. Soc. Rev.* **2007**, *36*, 367–377.
(29) Sessler, J. L.; Melfi, P. J.; Pantos, G. D. *Coord. Chem. Rev.* **2006**, *250*, 816–843.
(30) Casellato, U.; Sitran, S.; Tamburini, S.; Vigato, P. A.; Graziani, R. *Inorg. Chim. Acta* **1986**, *114*, 111–117.
(31) Sessler, J. L.; Vivian, A. E.; Seidel, D.; Burrell, A. K.; Hoehner, M.; Mody, T. D.; Gebauer, A.; Weghorn, S. J.; Lynch, V. *Coord. Chem. Rev.* **2001**, *216−217*, 411–434.
(32) Szigethy, G.; Raymond, K. N. *Inorg. Chem.* **2009**, *48*, 11489–11491.
(33) Szigethy, G.; Raymond, K. N. *Inorg. Chem.* **2010**, *49*, 6755–6765.
(34) Xu, J.; Raymond, K. N. *Inorg. Chem.* **1999**, *38*, 308–315.
(35) Szigethy, G.; Raymond, K. N. *Chem.—Eur. J.* **2011**, *17*, 1818–1827.
(36) Durbin, P. W.; Kullgren, B.; Ebbe, S. N.; Xu, J.; Raymond, K. N. *Health Phys.* **2000**, *78*, 511–521.
(37) Templeton, D. H.; Zalkin, A.; Ruben, H.; Templeton, L. K. *Acta Crystallogr., Sect. C* **1985**, *C41*, 1439–1441.
(38) Casellato, U.; Vigato, P. A.; Tamburini, S.; Graziani, R.; Vidali, M. *Inorg. Chim. Acta* **1983**, *72*, 141–147.
(39) Casellato, U.; Guerriero, P.; Tamburini, S.; Vigato, P. A.; Graziani, R. *J. Chem. Soc., Dalton Trans.* **1990**, 1533–1541.
(40) Andersen, O. *Chem. Rev.* **1999**, *99*, 2683–2710.
(41) Akine, S.; Taniguchi, T.; Nabeshima, T. *Tetrahedron Lett.* **2001**, *42*, 8861–8864.
(42) Akine, S.; Taniguchi, T.; Nabeshima, T. *J. Am. Chem. Soc.* **2006**, *128*, 15765–15774.
(43) Akine, S.; Sunaga, S.; Taniguchi, T.; Miyazaki, H.; Nabeshima, T. *Inorg. Chem.* **2007**, *46*, 2959–2961.
(44) Gallant, A. J.; Hui, J. K.-H.; Zahariev, F. E.; Wang, Y. A.; MacLachlan, M. J. *J. Org. Chem.* **2005**, *70*, 7936–7946.
(45) Garrett, T. M.; Cass, M. E.; Raymond, K. N. *J. Coord. Chem.* **1992**, *25*, 241–253.
(46) Rodgers, S. J.; Ng, C. Y.; Raymond, K. N. *J. Am. Chem. Soc.* **1985**, *107*, 4094–4095.
(47) Jurchen, K. M. C.; Raymond, K. N. *Inorg. Chem.* **2006**, *45*, 1078–1090.
(48) Gramer, C. J.; Raymond, K. N. *Inorg. Chem.* **2004**, *43*, 6397–6402.
(49) Jurchen, K. M. C.; Raymond, K. N. *J. Coord. Chem.* **2005**, *58*, 55–80.
(50) D'Aleo, A.; Xu, J.; Moore, E. G.; Jocher, C. J.; Raymond, K. N. *Inorg. Chem.* **2008**, *47*, 6109–6111.
(51) Sofen, S. R.; Abu-Dari, K.; Freyberg, D. P.; Raymond, K. N. *J. Am. Chem. Soc.* **1978**, *100*, 7882–7887.
(52) Scarrow, R. C.; Riley, P. E.; Abu-Dari, K.; White, D. L.; Raymond, K. N. *Inorg. Chem.* **1985**, *24*, 954–967.
(53) Riley, P. E.; Abu-Dari, K.; Raymond, K. N. *Inorg. Chem.* **1983**, *22*, 3940–3944.
(54) Xu, J.; Weisenhunt, D. W., Jr.; Veeck, A. C.; Uhlir, L. C.; Raymond, K. N. *Inorg. Chem.* **2003**, *42*, 2665–2674.
(55) Xu, J.; Franklin, S. J.; Whisenhunt, D. W. J.; Raymond, K. N. *J. Am. Chem. Soc.* **1995**, *117*, 7245–7246.
(56) Xu, J.; O'Sullivan, B.; Raymond, K. N. *Inorg. Chem.* **2002**, *41*, 6731–6742.
(57) Xu, J.; Radkov, E.; Ziegler, M.; Raymond, K. N. *Inorg. Chem.* **2000**, *39*, 4156–4164.
(58) Gorden, A. E. V.; Shuh, D. K.; Tiedemann, B. E. F.; Wilson, R. E.; Xu, J.; Raymond, K. N. *Chem.—Eur. J.* **2005**, *11*, 2842–2848.
(59) Committee on Cesium Processing Alternatives for High-Level Waste at the Savannah River Site; Board on Radioactive Waste Management; Board on Chemical Sciences and Technology; National Research Council *Alternatives for High-Level Waste Salt Processing at the Savannah River Site*; National Academies Press: Washington, DC, 2000.

(60) Committee on Disposition of High-Level Radioactive Waste Through Geological Isolation; Board on Radioactive Waste Management; National Research Council *Disposition of High-Level Waste and Spent Nuclear Fuel; The Continuing Societal and Technical Challenges*; National Academies Press: Washington, DC, 2001.
(61) Karpishin, T. B.; Stack, T. D. P.; Raymond, K. N. *J. Am. Chem. Soc.* **1993**, *115*, 182–192.
(62) Xu, J.; Durbin, P. W.; Kullgren, B.; Raymond, K. N. *J. Med. Chem.* **1995**, *38*, 2606–2614.
(63) Mullen, L.; Gong, C.; Czerwinski, K. R. *J. Radioanal. Nucl. Chem.* **2007**, *273*, 683–688.
(64) Martell, A. E.; Smith, R. M. *Critical Stability Constants*; Plenum: New York, 1977; Vol. 5.
(65) Szabó, Z.; Grenthe, I. *Inorg. Chem.* **2000**, *39*, 5036–5043.
(66) *SAINT: SAX Area-Detector Integration Program*, V.6.40; Bruker Analytical X-ray Systems, Inc.: Madison, WI, 2003.
(67) *SAINT: SAX Area-Detector Integration Program*, V.4.024; Siemens Industrial Automation, Inc.: Madison, WI, 1995.
(68) *XPREP, Part of SHELXTL Crystal Structure Determination Package*, V.6.12; Bruker Analytical X-ray Systems, Inc.: Madison, WI, 2001.
(69) *SADABS: Bruker Nonius Area Detector Scaling and Absorption*, V.2.05; Bruker Analytical X-ray Systems, Inc.: Madison, WI, 2003.
(70) *SHELXTL, SHELXTL Crystal Structure Determination Package*, V.5.10; Bruker Analytical X-ray Systems, Inc.: Madison, WI, 1997.
(71) Gans, P.; O'Sullivan, B. *Talanta* **2000**, *51*, 33–37.
(72) National Instruments Corp.; Bishop, R. H. *LABVIEW*, version 8.0; Pearson Prentice Hall: Upper Saddle River, NJ, 2007.
(73) Gans, P.; Sabatini, A.; Vacca, A. *Ann. Chim.* **1999**, *89*, 45–49.
(74) Brown, P. L. *Radiochim. Acta* **2002**, *90*, 589–593.
(75) Alderighi, L.; Gans, P.; Ienco, A.; Peters, D.; Sabatini, A.; Vacca, A. *Coord. Chem. Rev.* **1999**, *184*, 311–318.
(76) Gans, P. *HySS2*; University of Leeds: Leeds, U.K., 2000.